DESIGN AND TESTING OF AN MR DRUM ROTARY DEVICE TO ACHIEVE A VARIABLE EFFECTIVE COMPLIANCE TRANSMISSION

A Thesis

Presented in Partial Fulfillment of the

Requirements to Graduate 'with Distinction' at

The Ohio State University

By

Kyle Matthew Sabatka

* * * * *

The Ohio State University

2006

Approved by

Dr. Eric Westervelt, Advisor _____

Dr. James Schmiedeler, Co-Advisor _____

Advisors

ABSTRACT

The goal of this work was to compliment previous research that had been conducted to validate the concept of achieving a variable compliance transmission using a parallel combination of a magnetorheological (MR) fluid damper and a compliant element, together acting in series with an actuator. Two primary benefits of realizing such a system are identified: 1) the potential to achieve safer human-robot interactions while maintaining precise position control, and 2) the potential to produce a multi-pedal robot capable of achieving efficient locomotion at various speeds. A prototype transmission was previously built and tested to demonstrate such benefits.

Backlash in the prototype system proved to be problematic in conclusively demonstrating the potential benefits of using an MR rotary device to achieve an effectively compliant transmission. Specifically, position profiles were performed during which an end-effector was accelerated from rest to constant velocity, and then decelerated back to rest. The system demonstrated precise position control during every phase of the motion (e.g. acceleration, constant velocity, and deceleration) but never all in a single test. Depending on how the starting position of the damper body was chosen with respect to the backlash in the system, the body would inevitably rotate significantly relative to the shaft (input) during either the acceleration or deceleration phase, causing position error. Therefore, it

was necessary to design, build, and test a new MR rotary device, free of backlash to show that precise positioning could indeed be accomplished.

A new MR rotary device was designed and implemented into the previous system. Tests similar to those conducted with the previous MR device were performed to so that the new system could be compared to the former. Most importantly, the new system was able demonstrate precise position control throughout every phase of a motion profile during a single test. The position error was limited to 0.02 degrees of relative rotation between the damper body and shaft during a single trajectory. The results complimented those of the original prototype to conclusively demonstrate the potential benefits of using an MR rotary device to achieve a variable compliance transmission, especially for the case of achieving precise positioning during high magnitude acceleration and deceleration phases.

Dedicated to Lindsey and my family for their continued grace and support

ACKNOWLEDGMENTS

I would like to thank my advisor, Dr. Westervelt, and co-advisor, Dr. Schmiedeler, for giving me the opportunity to work on this project.

TABLE OF CONTENTS

CHAPTER 1: INTRODUCTION **1**

1.1 Objective **1**

1.2 Motivation **1**

1.3 Background **2**

1.4 Literature Review **4**

CHAPTER 2: EXPERIMENTAL APPARATUS **9**

2.1 Design of New MR Rotary Device **9**

2.1.1 Development of Design Equations *9*

2.1.1a Mechanical Requirements *10*

2.1.1b Electro-magnetic Circuit Requirements *11*

2.1.2 Preliminary Design Procedure *14*

2.1.3 MR Drum Device Components *16*

2.1.3a Outer Casing *17*

2.1.3b Aluminum Flanges *18*

2.1.3c Aluminum Shaft *19*

2.1.3d Steel Spool *20*

2.1.3e MR Foam and Fluid *21*

2.1.3f Slip Ring *22*

2.1.3g Magnet Wire *23*

2.2 Assembly of MR Device **23**

CHAPTER 3: PRELIMINARY TESTING 25

3.1 Static Calibration 25

3.1.1 Static calibration test procedure 26

3.1.2 Static calibration test results 28

3.2 Dynamic Calibration 33

3.2.1 Dynamic calibration test procedure 35

3.2.2 Dynamic calibration test results 36

3.3 Control of Velocity Profile Motion with Constant Damping 45

3.3.1 Control Scheme for Constant Damping Conditions 46

3.3.2 Test Procedure for Constant Damping Conditions 47

3.3.3 Results from Constant Damping Experiments 48

3.4 Control of Velocity Profile Motion with Variable Damping 50

3.4.1 Setup 52

3.4.2 Procedure for Velocity Profile Tests with Zero Applied Damper Current .. 53

3.4.3 Results of the Velocity Profile Tests with Zero Applied Damper Current ... 55

3.4.4 Procedure for the Velocity Profile Tests with Cubic Applied Damper Current 56

3.4.5 Results of the Velocity Profile Tests with Cubic Applied Damper Current 58

3.5 Impact Testing 58

3.5.1 Impact Test Setup 59

3.5.2 Impact Test Procedure 59

3.5.3 Impact Test Results 59

CHAPTER 4: CONCLUSIONS 63

4.1 Summary of Results 63

4.2 General Conclusions 66

4.3 Future Work 66

APPENDICES 68

Appendix A 69

Appendix B 75

Appendix C 78

Appendix D 79

LIST OF REFERENCES 85

LIST OF FIGURES

Figure 2.1: cross-section of MR drum device 10

Figure 2.2: Yield stress vs. magnetic field strength 13

Figure 2.3: Magnetic flux density vs. magnetic field strength 14

Figure 2.4: Cross-section of MR rotary device 16

Figure 2.5: Outer casing of MR drum 17

Figure 2.6: Aluminum flange 18

Figure 2.7: Aluminum Shaft 19

Figure 2.8: Steel spool 20

Figure 2.9: MR foam on spool 21

Figure 2.10: Slip ring with accessories and mounting diagram 22

Figure 2.11: Assembled MR system 23

Figure 2.12: Inner Chamber of MR system 24

Figure 3.1: Setup for static calibration tests 26

Figure 3.2: Static torque-current plot for increasing trials (new system) 29

Figure 3.3: Static torque-current plot for increasing trials (Bunting 2005) 29

Figure 3.4: Torque-current plot demonstrating hysteresis (new system) 32

Figure 3.5: Torque-current plot demonstrating hysteresis (Bunting 2005) 32

Figure 3.6: Setup for dynamic calibration (new system) 34

Figure 3.7: Setup for dynamic calibration (Bunting 2005) 34

Figure 3.8: Irregular motor command signal (Bunting 2005)..... 36

Figure 3.9: Irregular motor commands for new system..... 38

Figure 3.10: Damper torque-current data for 10rpm motor speed (new system) 40

Figure 3.11: Damper torque-current data for 10rpm motor speed (Bunting 2005) 41

Figure 3.12: Damper hysteresis, 10rpm motor speed (new system)..... 42

Figure 3.13: Damper hysteresis, 10 rpm motor speed (Bunting 2005)..... 43

Figure 3.14: Speed independence of torque-current curves (new system) 44

Figure 3.15: Speed independence of torque-current curves (Bunting 2005) 44

Figure 3.16: Setup for velocity profile tests..... 46

Figure 3.17: Position and velocity profiles 47

Figure 3.18: Damper current input with cubic curves 51

Figure 3.19: Five repeatable trials, acceleration with zero applied current 53

Figure 3.20: Eight repeatable trials, acceleration with zero applied current 54

Figure 3.21: Overshoot comparison for zero current and optimum current (new system)...

..... 56

Figure 3.22: Overshoot comparison for zero current and optimum current (Bunting 2005)

..... 57

Figure 3.23: Comparison of impact forces for varying cruising velocities (new system)....

..... 61

Figure 3.24: Comparison of impact forces for varying cruising velocities (Bunting 2005).

..... 61

LIST OF TABLES

Table 2.1: Specifications for slip ring model 205 22

Table 3.1: Percent reduction in impact loads for various cruising velocities (new system) 62

Table 3.2: Percent reduction in impact loads for various cruising velocities 62

Table B1 75

Table B2: 76

CHAPTER 1: INTRODUCTION

1.1 Objective

The purpose for designing, building, and testing a variable effective compliance transmission using a magnetorheological (MR) drum device was to compliment previous research with a similar device, of which the ultimate goal was to demonstrate increased safety during motion without sacrificing precision motion control.

1.2 Motivation

The primary driver of the research was the need to create a system free of significant backlash that could be tested and compared to previous results obtained using an MR disk clutch system that exhibited undesirable backlash. Backlash in the previous system proved to be problematic in obtaining conclusive results to demonstrate the stated purpose of the previous research.

An experimental apparatus and control scheme was previously developed by Bunting in order to test a variable effective compliance transmission that utilized a commercial MR disk clutch (model MRB-2107-3) designed and built by the Lord Corporation. During preliminary testing, however, a significant amount of backlash was observed in the disk clutch. The amount of backlash was determined to be approximately two degrees. The backlash in the system hindered testing and made it especially difficult to conclusively

demonstrate the device's ability to achieve precise positioning by effectively eliminating compliance. It was therefore necessary to design and build another MR rotary device, free of backlash that could be incorporated in the previously designed apparatus, and utilize the same control scheme so that similar testing could be performed.

By demonstrating comparable or improved performance to that of the system incorporating the MR disk rotary device, results from the transmission incorporating the newly designed MR drum rotary device would then further substantiate the use of a variable effective compliance system that specifically incorporates an MR system, as outlined by Westervelt (2004). The research is also primarily motivated by the work of Bicchi and Tonietti (2004) that describes the need to incorporate a variable compliance transmission in robots to achieve precise motion control at high speeds while simultaneously increasing safety.

1.3 Background

Variable effective compliance was achieved by placing a parallel combination of an MR rotary device and torsion spring in series with a shaft connected to a motor. Compliance is defined as the inverse of stiffness. The compliance was effectively varied by changing the effective shear stress properties of the fluid within the MR device.

The fluids found within MR devices contain micron-sized ferrous particles, which give such devices their unique characteristics. The fluids are typically oil or water based. In the presence of a magnetic field, the ferrous particles align and significantly increase the

apparent viscosity and shear stress of the fluid. When the magnetic field is removed, the ferrous particles float freely and yield an apparent viscosity similar to that of the fluid. This ultimately leads to higher holding torques or increased damping in MR rotary devices that serve as clutches and/or brakes, respectively.

It should be understood that MR rotary devices can operate both as a clutch and a brake depending on whether or not they are transmitting energy into or away from the output. When operating as a clutch, torque is transmitted from a shaft (usually connected to a motor), through the MR fluid and output to a mechanical component in order to transmit power and cause rotation of this last component. When the MR device is used as a brake, the mechanical component at the output is typically rotating relative to the shaft and a resistive torque is applied through the MR fluid in order to dissipate the kinetic energy of the output component (provide damping). The MR rotary device used for the purposes of this research operated both as a clutch and a brake depending on the nature of the experiments.

It is also necessary to define the term ‘end-effector,’ because of its extensive use throughout the text. An ‘end-effector’ can be understood as the last link of a robotic device. By identifying the end-effector, one can understand the ultimate purpose of the robotic device. For example, cutting and welding tools are often found on industrial robotic manipulators (Bunting 2005). For the purposes of this research, the position, velocity, and trajectory of the end-effector were used to relate and control the motion of the entire system.

1.4 Literature Review

The potential safety benefits of introducing compliance into a robotic system and the various means by which this could be accomplished were thoroughly discussed by Bicchi and Tonietti (2004). Numerous robotic system arrangements have been proposed to introduce compliance and reduce the amount of inertia coupled to the end-effector. One such example is a series-elastic actuator. Such a system provides greater shock tolerance, which reduces the risk of injury and damage in the environment, and has the capacity to store energy (Pratt and Williamson 1995). Though system compliance addresses safety concerns, other challenges are introduced such as undesired oscillatory motion and the subsequent design and control issues.

The challenges posed by introducing compliance into robotic systems led Bicchi and Tonietti (2004) to suggest the concept of a variable stiffness transmission (VST). If such a system existed, compliance could be changed as needed during the execution of an end-effector's motion profile. A more rigid system was required in order to transmit the high torques needed to maintain precise positioning during the acceleration and deceleration phases of the motion. However, a more compliant system was sufficient for precise motion control during the intermittent constant velocity phase and provided the added benefit of increased safety in the event of an impact (Bicchi and Tonietti 2004).

A potential VST system is described by Morita and Sugano (1995) that incorporates a leaf spring – slider system in the joint of a robotic finger. Effective damping is accomplished using a brake. Research demonstrated more precise motion by attenuating

oscillations through the use of the brake. However, practical implementation of the complicated control scheme and multiple system components seemed to be infeasible.

Another possible means of implementing a VST system into a robotic manipulator was proposed by Laurin-Kovitz (1991). Their work focused on controlling and varying passive impedance elements. The passive elements included an antagonistic pair of non-linear springs and a damper, while active compliance was accomplished using control schemes. Using passive elements served to increase system stability and the active control allowed for more versatility. An appropriate controller would allow the stiffness and damping in the system to be varied, however, the non-linearity of the springs would make practical implementation in a robotic manipulator difficult.

One particular methodology for achieving VST in robotic systems is antagonistic muscle actuation similar to that of the human body (Bicchi 2001). For example, simultaneously flexing one's bicep and tricep muscles causes the joint at the elbow to become stiff. Bicchi and Tonietti suggested the use of McKibben actuators to accomplish VST in a robotic arm (2001). McKibben actuators are pneumatic devices that were originally developed to research artificial limbs (Chou and Hannaford 1996). Some hindrances to practical implementation of such actuators in robotic include their need for a pressure source and slow response time (Bicchi and Tonietti 2004).

Electrorheological (ER) fluid devices have been used to effectively control vibration in transmissions (Takesue 1999). The ER damper was placed in series between the drive

and end-effector to resist motion and attenuate oscillations. ER dampers are activated when an electric flux passes through the ER fluid and increases its apparent viscosity. Though the ER device improved the system performance for the specific application, large electric fields are required to activate the damper (Morita and Sugano 1995). Accordingly, excessive size and weight would be a concern for implementation in a manipulator.

A variable effective compliance transmission using a parallel combination of a spring and an MR damper was developed by Kim *et al.* for use in a Public Service Robot at the Korea Institute of Science and Technology (2002, 2004). The design incorporated passive torsion springs to introduce compliance at the joints so that the risk of injury would be mitigated in the event of an incidental impact with a human being. The relative angular position between the out drive and link that resulted due to spring displacements was differentiated calculate the relative velocity. The current to the MR damper was chosen depending on the observed relative velocity to realize a desired damping ratio and minimize oscillations. Impact testing was conducted for various linear velocities. However, the choice of damping during the experiments was not discussed. Moreover, it is unclear whether the damping was varied during a single trajectory. The results of the research demonstrated the system's ability to reduce oscillations using sufficient damping.

In order to create a VST system, a research schedule for a variable effective compliance transmission with an MR damper was outlined (Westervelt *et al.* 2004). A parallel

spring-damper configuration was conceptualized for a linear transmission system. The damping ratio of the MR device could be varied by changing the applied magnetic field, and effectively vary the compliance. So, incorporating such a device into a legged robot would enable the robot to absorb impacts caused by contact with the ground as well as achieve high speed locomotion by becoming more rigid. Furthermore, rigid motions would be desirable during acceleration phases to maintain precise positioning, while effectively varying the compliance would address safety issues when the device is traveling at a constant velocity.

Testing of a variable effective compliance system that incorporated an MR rotary device was conducted by Bunting (2005) to validate the concepts presented by Westervelt *et al.* (2004). Bunting used a control scheme to vary the current applied to the MR damper in order to maintain precision control while increasing safety. High currents were commanded during the acceleration and deceleration phases when high torque transmission was required to maintain precise positioning. Low currents were applied to the damper during the constant velocity phase of the motion when low torque transmission was required to maintain precise position control. Safety was increased because the system was effectively rigid only during the low velocity, high acceleration phase and effectively compliant during the high velocity motion. The presence of backlash in the rotary device, however, proved to be problematic in conclusively validating the intended purpose of the device. Specifically, precise motion control could only be achieved during either the acceleration or deceleration phase of a single trajectory, but never during both phases.

The project described throughout the text was completed to compliment the research conducted by Bunting (2005) in order to further validate the concepts presented by Westervelt *et al.* (2004). A new MR rotary device was designed and built so that the tests that were performed on the previous system could be repeated on a system lacking significant backlash.

CHAPTER 2: EXPERIMENTAL APPARATUS

The experimental apparatus used by Bunting (2005) to test the previous system was essentially left unchanged except for the use a newly designed MR device. Since Bunting provides a detailed explanation of the components used in the experimental apparatus, this chapter focuses primarily on the design of the new MR system and will highlight any changes that were made to the previous configuration of the apparatus. Specifications for particular components will be discussed as needed.

2.1 Design of New MR Rotary Device

The design of the MR rotary device was based on the procedures involved two parts. The first part involved the development of the theoretical design equations. A MATLAB script was then written that incorporated the design equations in order to automate part of the design procedure. The second part was the detailed design of the individual components that would make up the MR rotary system.

2.1.1 Development of Design Equations

The new MR device was designed to have the same holding torque (50in-lb) as the previous system. In order to provide the specified holding torque, both mechanical and electro-magnetic circuit requirements had to be satisfied.

2.1.1a Mechanical Requirements

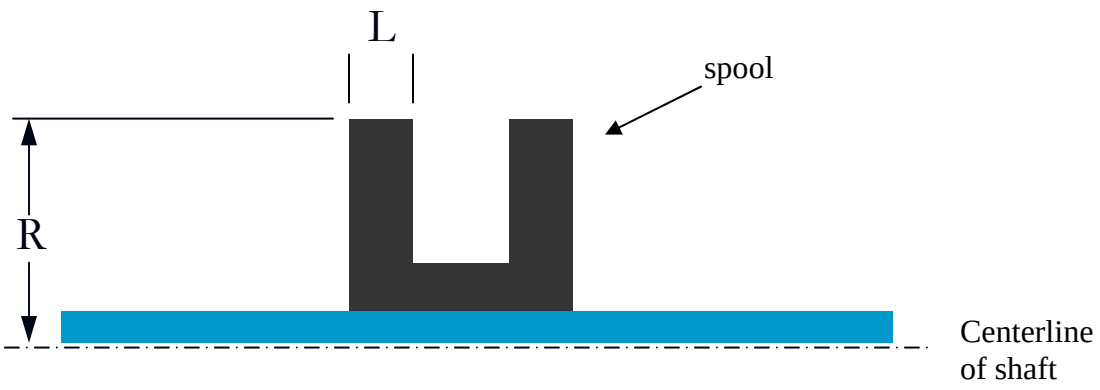

Figure 2.1: cross-section of MR drum device

The simple diagram representing the cross-section of an MR drum device is shown in Figure 2.1, and highlights the key parameters used in the development of the mechanical design equation. 'R' represents the radius of the spool and 'L' represents the length of the portion of the spool indicated in the figure. The outer edge of the spool transmits torque through MR fluid to an outer casing (a.k.a. drum). The primary mechanical equation is listed below and serves as the starting point for the mechanical part of the design.

$$\tau = \tau_y + \eta \frac{d\gamma}{dt} \qquad (2.1)$$

$\tau \doteq$ shear stress developed within MR fluid
$\tau_y \doteq$ dynamic yield stress
$\eta \doteq$ plastic viscosity
$\frac{d\gamma}{dt} \doteq$ shear rate

The goal of the design is to achieve a specified holding torque, so the shear rate is assumed to be zero. Thus, the shear stress developed within the MR fluid is set equal to the dynamic yield stress:

$$\text{holding torque} \rightarrow \frac{d\gamma}{dt} = 0 \rightarrow \tau = \tau_y \qquad (2.2)$$

The holding torque is equal to the radial force multiplied by the radius:

$$T = FR \qquad (2.3)$$

Since the MR fluid contacts only the outer radius of the spool and not the narrow center portion, the radial force transmitted by the MR fluid is equal to the dynamic yield stress multiplied by the area of the outer portions of the spool:

$$F = \tau_y A \qquad (2.4)$$

Also based on the geometry, the area of the outer portions of the spool that is in contact with the MR fluid is given as:

$$A = 4\pi RL \qquad (2.5)$$

Combining equations (2.2) through (2.5), the mechanical design equation is obtained that relates the radius and length of the spool to the dynamic yield stress of the MR fluid and the holding torque:

$$R^2 L = \frac{T}{4\pi\tau_y} \qquad (2.6)$$

Lord Corporation provides the dynamic yield stress for various MR fluids. Thus, since the holding torque is specified and the dynamic yield stress of the MR fluid can easily be obtained or estimated, the radius and length of the spool are the only unknowns remaining in the design equation. So, one could specify ‘R’ or ‘L’ and the equation would give the value for the other parameter.

2.1.1b Electro-magnetic Circuit Requirements

The primary electro-magnetic circuit equation is listed below and serves as the starting point for the development of the second design equation. It states that the number of turns of the electrical conductor multiplied by the amount of current traveling through the conductor is equal to the magnetic flux traveling through the MR fluid multiplied by the total reluctance of the magnetic circuit:

$$NI \doteq \phi(\text{Reluctance}) \qquad (2.7)$$

$N \doteq$ number of turns
$I \doteq$ electrical current
$\phi \doteq$ magnetic flux
$\text{Reluctance} = \sum_{i=1}^{n} \text{Rel}_i$

The total reluctance is simply equal to the sum of all the individual reluctances within magnetic circuit:

$$\text{Rel}_i = \frac{L_i}{\mu_i A_i} \qquad (2.8)$$

$L_i \doteq$ length of flux path
$\mu_i \doteq$ permeability
$A_i \doteq$ cross-sectional area perpendicular to flux

The magnetic flux traveling through the MR fluid is also equal to the magnetic flux density, B, multiplied by the cross-sectional area of the MR fluid, A_{MR}, that is perpendicular to the flux path:

$$\phi = BA_{MR} \qquad (2.9)$$

Combining equations (2.7), (2.8), and (2.9) yields the second design equation:

$$NI = \phi B A_{MR} \sum_{i=1}^{n} \mathrm{Rel}_i \qquad (2.10)$$

Again, using known properties of the particular MR fluid, the design equation can be reduced to two unknowns. The total reluctance of the magnetic circuit can be found using equation (2.8). The flux density, B, can be determined as follows. First, locate the maximum yield stress on the 'Yield stress vs. magnetic field strength' plot for the specific MR fluid. Next, look at the x-axis to determine the corresponding magnetic field strength value, H. Using the magnetic field strength determined from Figure 2.2, Figure 2.3 can be used to determine the corresponding flux density value, B. Thus, the only remaining unknowns in equation (2.10) are the number of turns, N, and the electrical current, I. Depending on the available space for windings for the geometry of the MR device, the current carrying capacity of the wire, and maximum voltage capabilities of the power source, N or I can be selected and equation (2.10) will give the minimum value of the other parameter necessary to satisfy the electro-magnetic circuit requirements.

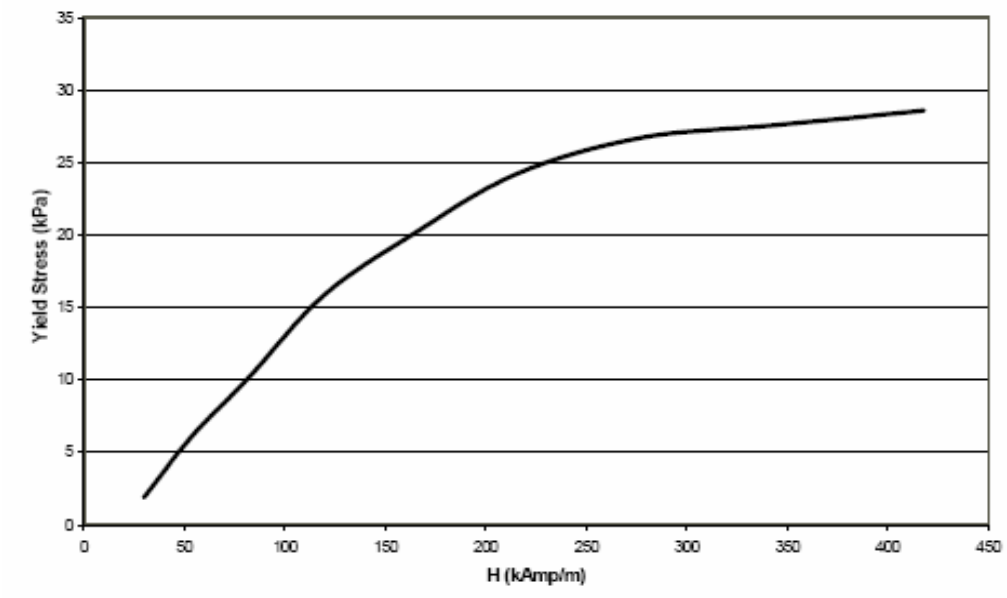

Figure 2.2: Yield stress vs. magnetic field strength (courtesy of Lord Corporation)

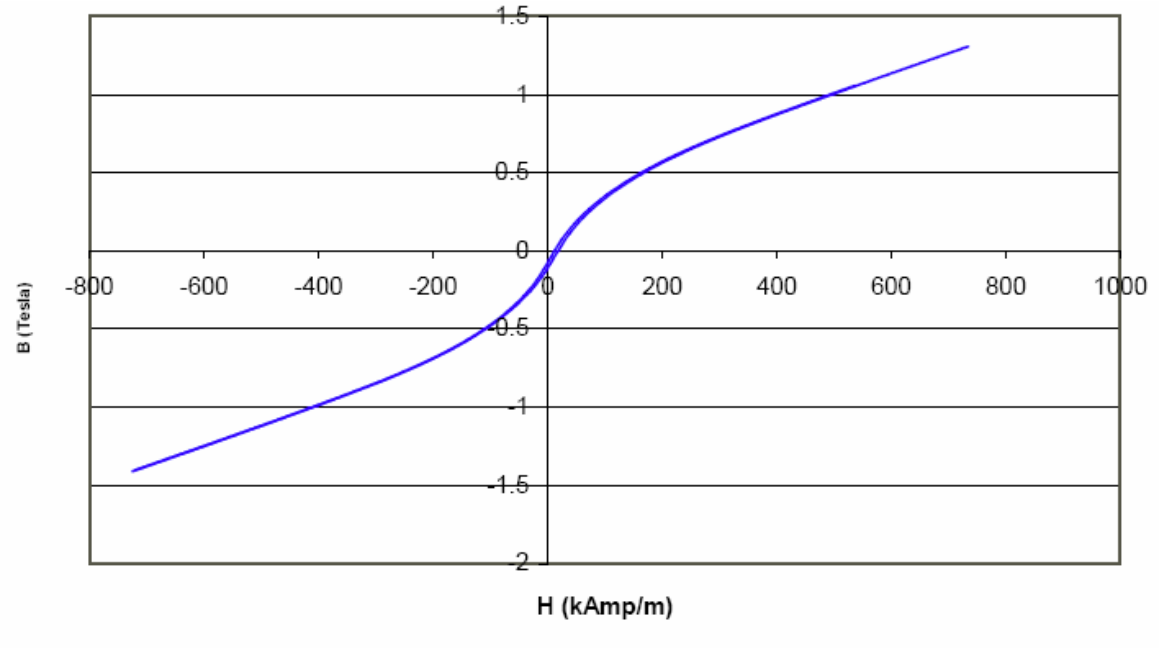

Figure 2.3: Magnetic flux density vs. magnetic field strength (courtesy of Lord Corporation)

2.1.2 Preliminary Design Procedure

The two primary design equations derived above were used to automate the design process using MATLAB. The list of inputs to the program included the desired holding torque, the desired length or radius of the spool, the flux density determined from the above plots, the shaft diameter, the thickness of the outer casing (output), and the desired saturation current value. Using the inputs as well as some other geometric relationships suggested by Ahmadkhanlou (2005) to parameterize the design process, the program output the length or radius of the drum, the number of turns necessary to satisfy the magnetic circuit requirements, and the maximum number of turns that could fit in the available space for various wire gauges.

The design of the new MR device began by choosing a value for the radius of the spool component of the system. Since it was expensive and wasteful to bore a solid piece of steel to create the outer steel casing (drum), it was decided to use a piece of schedule 80 (i.e. extra-heavy) steel pipe. The pipe could be easily and quickly machined to a given thickness. Also, extra-heavy pipe was chosen as opposed to standard pipe so that it could be machined and still be thick enough to allow a sufficient amount of magnetic flux through the steel. Since the new MR device was to fit into the original apparatus, the radius of the new system needed to be comparable to that of the previous device. Using the above criterion, the nominal size for the black pipe was chosen to be 3.5inches.

The pipe was to be machined to a reasonable thickness of 3/16", as suggested by Ahmadkhanlou (2005). The outside diameter and wall thickness for nominal 3.5inch pipe was listed in at www.pipevalves.com. Assuming the 3/16" wall thickness and some machining on both walls of the stock piece of pipe, the inner diameter of the outer casing was calculated. Between the spool and outer casing was foam that was to be used to contain the MR fluid (see Figure 2.4). The foam was provided by Dr. Gregory Washington's Smart Materials Laboratory at The Ohio State University and of a standard 3.1mm thickness. The gap length between the spool and the outer casing was chosen to be 2.7mm to ensure contact around the entire circumference of the device. Finally, knowing the inner diameter of the casing and the gap length, a value for the radius of the spool was obtained. The specific dimensions of components are discussed more thoroughly in later sections.

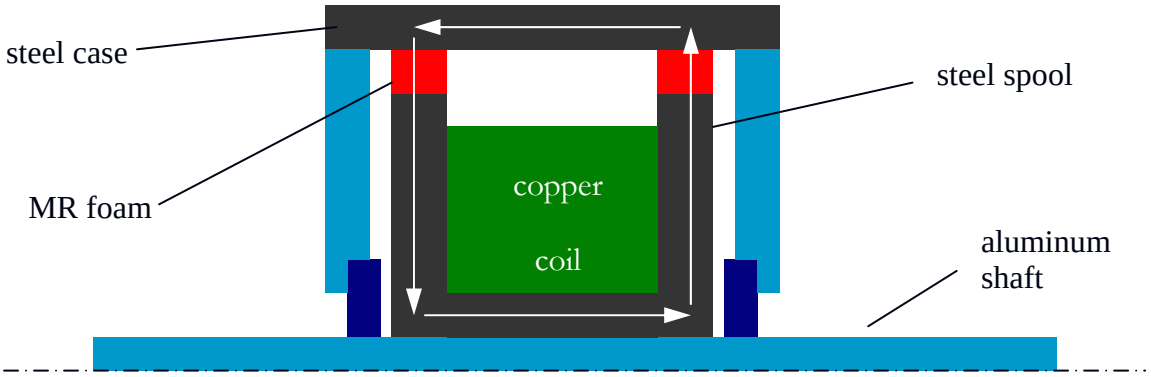

Figure 2.4: Cross-section of MR rotary device (drum configuration). Note: arrows represent the path of the magnetic flux.

The value of the radius of the spool was then input into the design program. The value of the dynamic yield stress input to the program was estimated by Ahmadkhanlou (2005) based on previous experience. The MATLAB script output a corresponding length of the spool that seemed reasonable but would require re-machining longer poly-carbonate frames in order to accommodate the added body length and prevent interference from occurring between various components. The script was used to determine that 26 - gauge wire would be necessary in order to fit the required number of turns in the available space. With the basic dimensions of the system established, the design of the specific components commenced.

2.1.3 MR Drum Device Components

The following components were used to assemble the new MR drum device and replace the previous system. The design of each component is discussed in the corresponding subsection.

2.1.3a Outer Casing

The outer casing had an outer diameter of 3.36 inches. As previously discussed, its radius was chosen so that the component could be machined from a piece of scrap schedule 80 black steel pipe. Four evenly spaced holes were drilled and tapped on the flat edges of the case so that it could be fixed to two aluminum flanges that rested on bearings mounted to an aluminum shaft. Steel was chosen due to its ferrous content through which magnetic flux easily passes. The component is shown below in Figure 2.5.

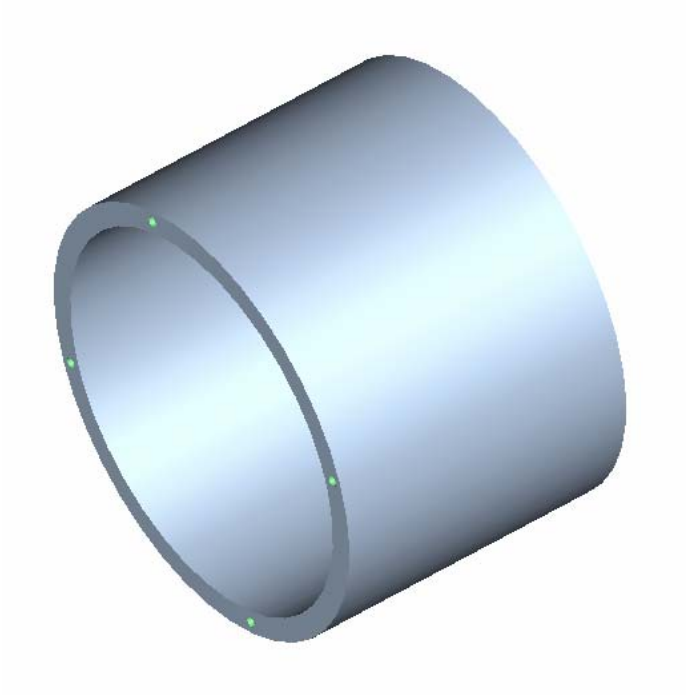

Figure 2.5: Outer casing of MR drum device

2.1.3b Aluminum Flanges

The aluminum flanges connected the outer casing to bearings that were mounted to the shaft. Aluminum was the material of choice for a number of reasons. It is light and minimizes inertia. It is sufficiently strong and is much less permeable than steel. This serves to prevent flux leakage. Also, six holes were drilled and tapped to the face of one of the flanges. The holes were for threaded studs that would be used to connect to the hollow shaft encoder that was part of the original experimental apparatus. The component is shown below in Figure 2.6. A hole was also threaded and tapped into the side of the other flange to accommodate the threaded rod that served as the end-effector

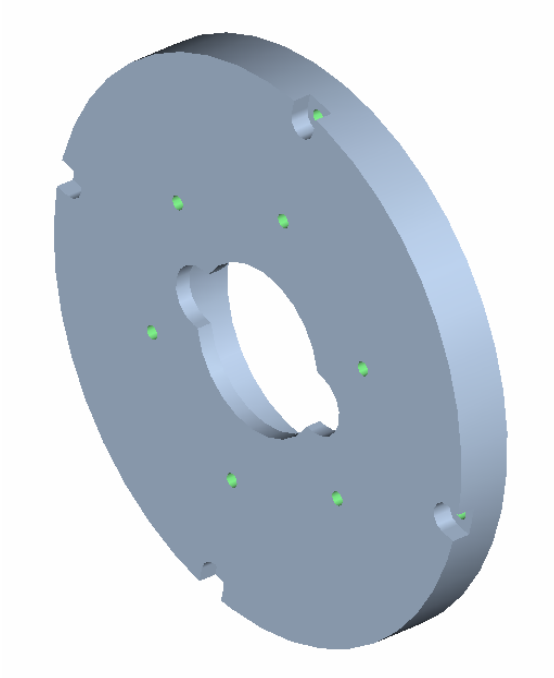

Figure 2.6: Aluminum flange

2.1.3c Aluminum Shaft

The overall length of the shaft was increased corresponding to the increase of the newly designed damper body as compared to the old system. The diameter of the shaft was chosen to be the same as that of the original system. A hole was drilled perpendicular and through the axis of the shaft so that a spring pin could fix the spool to the shaft. Also, a small groove was machined into the shaft to accommodate a snap ring to fix its horizontal position. A keyway was placed on one end of the shaft so that the shaft could be rigidly connected to the motor. The shaft was also bored along the axis for approximately half of the shaft length. This was done to allow copper wire leads to be fed from the winding around the spool, out through the center of the shaft to a slip ring. Aluminum was selected for its light weight, high strength, and low magnetic permeability. The shaft is shown in Figure 2.7.

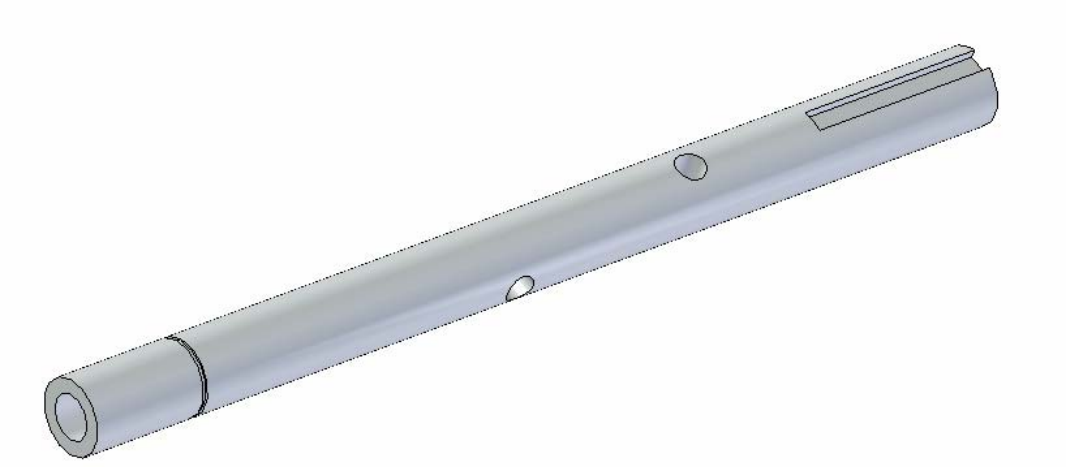

Figure 2.7: Aluminum Shaft

2.1.3d Steel Spool

The chosen dimension for the radius was explained earlier. The length of the drum was output from the design script. One end of the drum was made to extend out further than the other in order to drill a hole for a spring pin that fixed the drum to the aluminum shaft. A small circular ridge extended further from the protruding end in order to contact the inner race of a bearing and fix the horizontal position of the outer casing. The narrow space between the large circular sections of the spool accommodates the copper wire winding. Steel was chosen so that the magnetic circuit could be completed. A hole and groove were machined into one of the large circular sections in order to allow the ends of the copper wire to exit the narrow middle section and enter a hole in the shaft. A 3-D model of the drum is shown in Figure 2.8

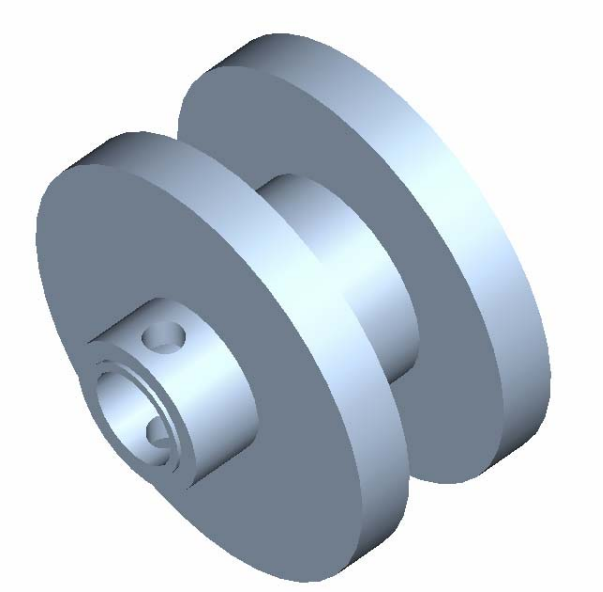

Figure 2.8: Steel spool

2.1.3e MR Foam and Fluid

The MR fluid was made in Dr. Gregory Washington's Smart Material Laboratory at The Ohio State University. The carrier fluid was a 10 cST silicone oil. The iron powder contained four micron to seven micron sized ferrous particles. The fluid contained approximately 5.4 parts of iron to one part oil, based on weight. The approximate dynamic yield stress was 40 kPa (Ahmadkhanlou 2005). The fluid was carried in 3.1mm thick foam. The foam prevented leakage while the pores were large enough to allow shearing of the fluid. This made for a simple yet clean design that did not need any kind of special mechanical seals. The foam was glued to the outer most surfaces of the spool and contacted the outer casing. A 3-D rendering of the foam glued to the steel spool is shown in Figure 2.9.

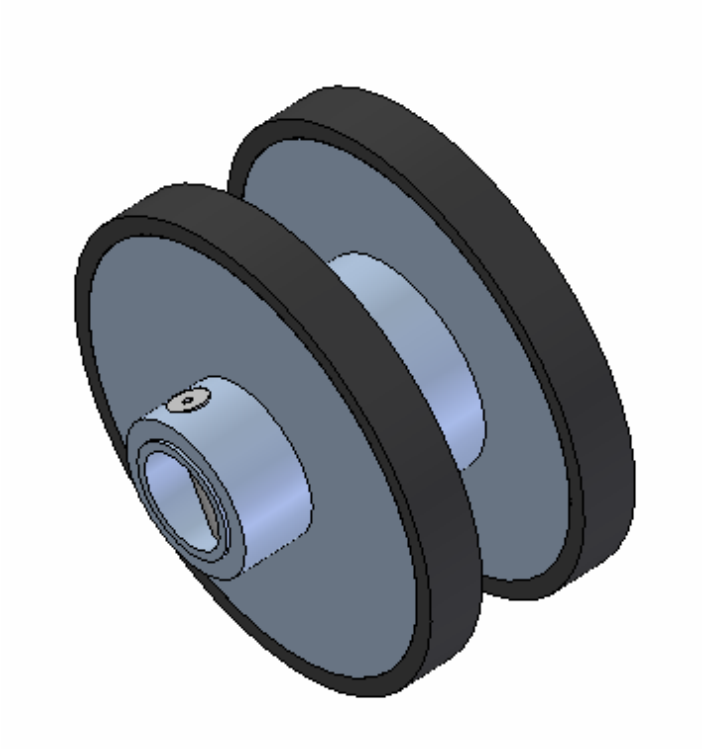

Figure 2.9: MR foam on spool

2.1.3f Slip Ring

In order to maintain simplicity and limit the chance of breaking wires in the case of continuous rotation of the system, a slip ring was incorporated into the design. The slip ring model 205 was purchased from Mercotac. The specifications for the slip ring are listed in Table 2.1. Additional accessories were required in order to implement the slip ring into the MR device. These included a two contact receptacle (model 592) and a two contact cap (model 595). The slip ring mounted to a bore in the shaft connected to the motor. The slip ring, accessories, and mounting diagram are shown below in Figure 2.10.

Table 2.1: Specifications for slip ring model 205

Model No.	Terminals	Voltage AC/DC	Amp Rating @240VAC	Max. Freq. MHz	Contact Resistance	Max. RPM	Temp Max. F (C) / Min. F (C)	Rotation Torque (gm-cm)	Circuit Separation
205	2	0-250	4	200	<1m Ω	2000	140 (60) /45(7)	75	>25M Ω

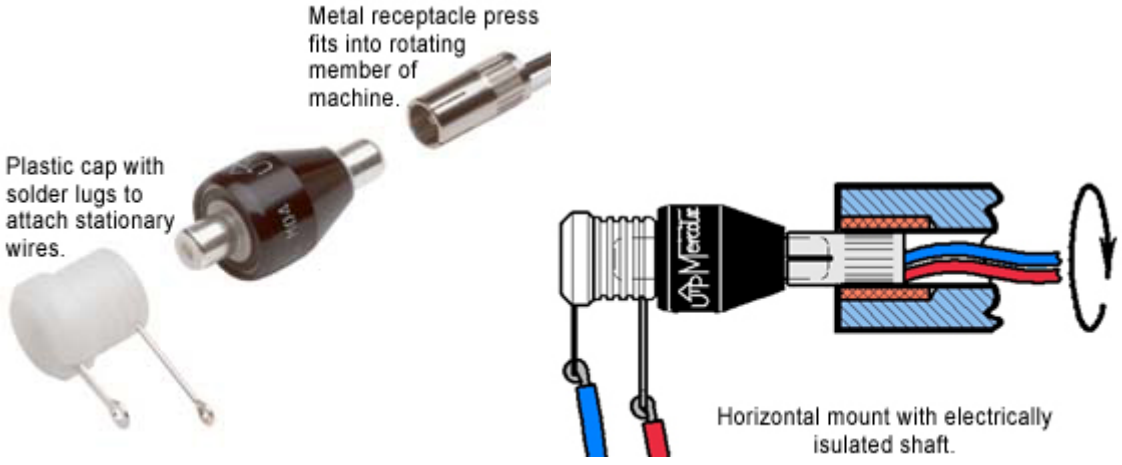

Figure 2.10: Slip ring with accessories and mounting diagram (table and figures courtesy of www.mercotac.com)

2.1.3g Magnet Wire

The copper wire that was wound about the steel spool (1210 total turns) and used to induce a magnetic field was purchased through McMaster-Carr. 3,000ft of the the 26 AWG “magnet wire” (part # 7588K55) was purchased. The copper wire was coated with clear enamel. The diameter of the wire and enamel was 0.018inches. The maximum temperature rating is 392 degrees Fahrenheit.

2.2 Assembly of MR Device

The final assembly is depicted in Figures 2.11 and 2.12. The shaft is rigidly keyed to the motor via a coupling. A snap ring prevents horizontal movement in the other direction. The steel spool is fixed to the aluminum shaft using a spring coupling. Ball bearings are pressed into the aluminum flanges. The inner races of the bearings contact the steel spool and a spacer that prohibit horizontal motion relative to the shaft. Finally, the outer casing is mounted between the aluminum couplings using threaded fasteners. The outer casing can rotate relative to the shaft because of the bearings.

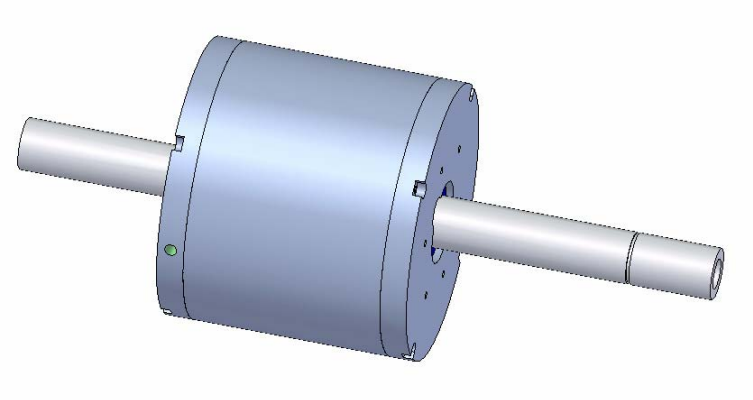

Figure 2.10: Assembled MR system

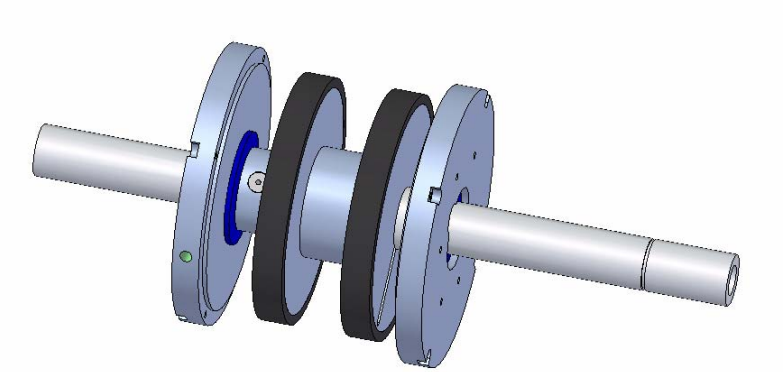

Figure 2.11: Inner Chamber of MR system

CHAPTER 3: PRELIMINARY TESTING

Prior to performing the experiments to validate the concept of the new drum clutch configuration versus the previous disk clutch configuration of the variable effective compliance transmission, it was necessary to characterize the behavior of the MR drum clutch and confirm that the control scheme previously developed by Bunting was also tenable for the new system. Four different sets of experiments were conducted. The first two sets involved static and dynamic calibration in order to relate the torque output of the system to the supplied electric current to the damper. The latter two sets of experiments used Bunting's control scheme and controller gains to execute a specific velocity profile with both constant and varying applied currents to the damper. The results of the velocity profile tests were compared to those obtained by Bunting (2005).

3.1 Static Calibration

In order to establish a holding torque-current relationship a static calibration was performed. The drum clutch was designed to operate linearly and output a torque of 50.0in-lb at an applied current of 1.25Amp. In order to perform the calibration, the shaft of the system was fixed to a table using a pair of V-blocks and C-clamps. A piece of all-thread-rod was inserted in two the outer body of the clutch and positioned horizontally over the edge of the table. Heavy steel wire was fed through a hole in the all-thread-rod located 2.5 inches from the axis of rotation. The wire was tied in a loop so that a metal

hanger capable of carrying weights could be attached to the system. Knowing the location of the hole through which the wire was fed allowed one to determine the corresponding holding torque based on the force applied. A power supply was connected to a slip ring so that current could be applied to the damper. The setup is shown in Figure 3.1.

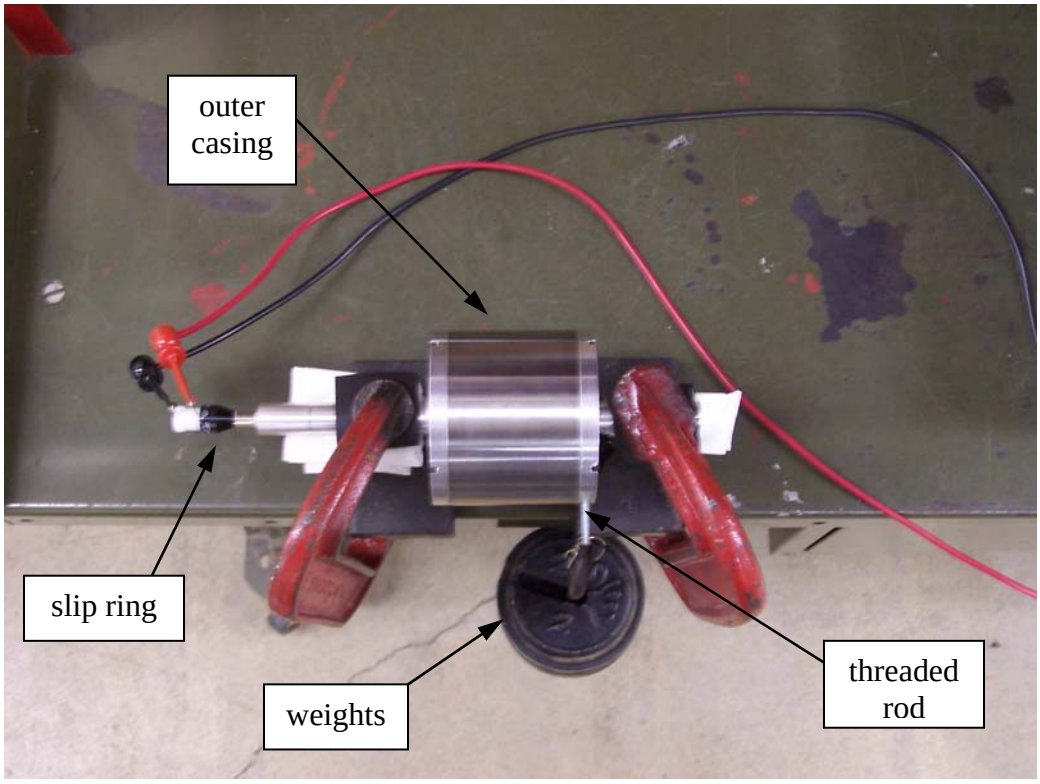

Figure 3.1: Setup for static calibration tests

3.1.1 Static calibration test procedure

Eight two-pound weights, three one-pound weights, and one one-pound weight hanger were used to apply torques to the system. With a relatively small current applied to the

damper the one-pound hanger was hung from the steel loop. The current was incrementally increased by 0.01 Amp until the clutch was able to support the load and maintain the threaded rod in a horizontal position. The current value was recorded as well as the applied torque due to the offset load from the hanger. It was important increase the current in small increments so that the smallest sufficient value could be identified. The process continued with individual weights being added to the hanger and the current incrementally increased by 0.01 Amp until the clutch could support the load. Though it was desired to test the clutch over its entire designed current range of 0 to 1.25 Amps, the experiment was limited by the maximum available voltage that could be supplied by the power source, which could no longer provide additional current due to resistance of the winding within the clutch. The corresponding current value for the maximum torque that could be supported by the clutch without exceeding the limits of the power supply was approximately 0.93 Amps. Three individual trials were performed testing the clutch over a range of 0 to 0.93 Amps.

In order to examine hysteresis effects two additional static calibration trials were performed that included both increasing and decreasing currents and weights. After the increasing portion of these trials (as described above) when the clutch was holding the torque at the current that was limited by the power supply, similar tests were conducted for decreasing current values. A two-pound weight was removed from the hanger and the current was incrementally decreased until the clutch could no longer maintain the applied torque. When the applied current became sufficiently small, the damper body rotated relative to the shaft and the threaded rod holding the weights could no longer be

maintained in a horizontal position. Bunting (Bunting) characterized this event as the breakaway point. When the horizontal position could no longer be maintained, the corresponding current and torque were recorded. The current was then incrementally increased until the same load could once again be supported. This current value was significantly higher than that obtained at the breakaway point. The corresponding current value was again noted. Finally, an individual weight was removed and the procedure was repeated until no weight remained on the hanger.

3.1.2 Static calibration test results

The results for the three increasing trials yielded similar results. The data for the trials are shown in Figure 3.2. As expected, the data exhibited a linear torque-current relationship. A linear curve with an initial value of zero torque at zero applied current was fit to the average of the three trials. The sensitivity of the clutch as determined from the linear fit was 41.4in-lb per 1.0Amp of current applied to the damper.

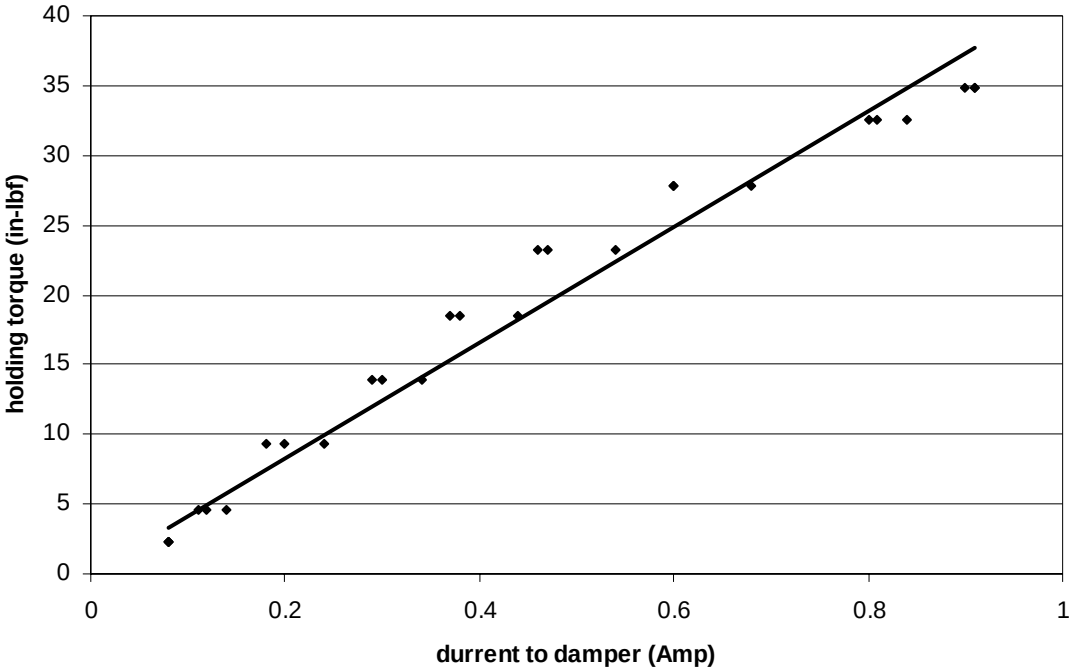

Figure 3.2: Static torque-current plot for increasing trials (new system)

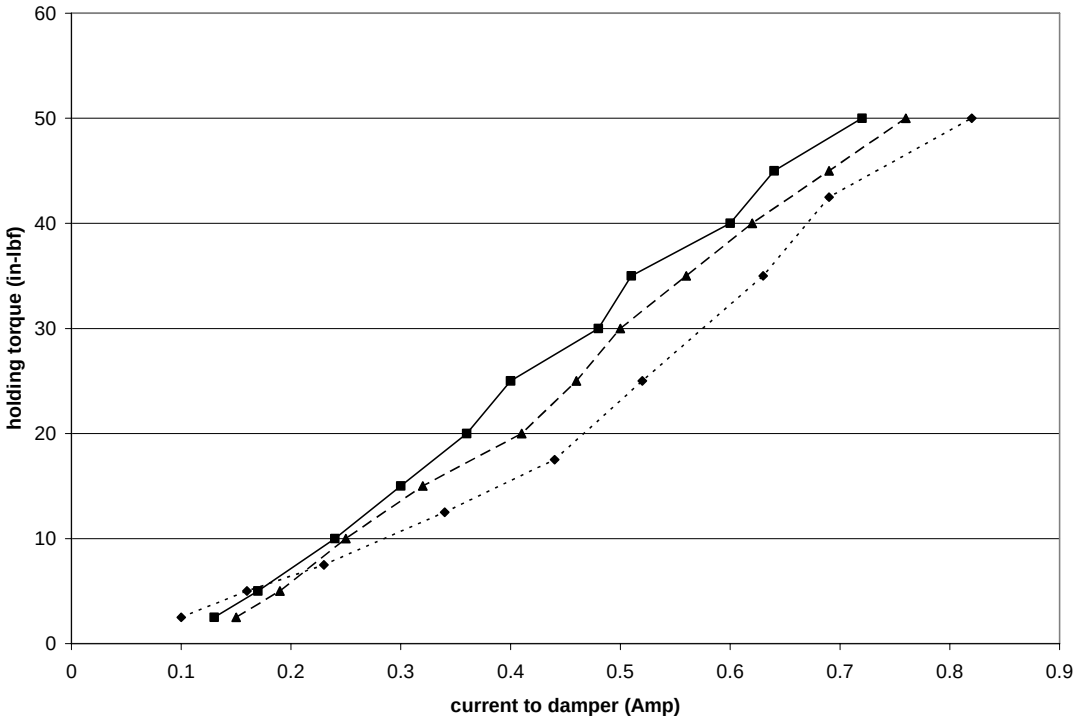

Figure 3.3: Static torque-current plot for increasing trials (Bunting 2005)

As previously mentioned, the clutch was designed to provide a maximum holding torque of 50.0in-lb at its designed saturation current of 1.25 Amps. Since the voltage limit of the power supply and the resistance of the winding in the system prevented the clutch from actually being tested at its saturation current, the sensitivity obtained from the linear fit curve was used to extrapolate this value. The maximum holding torque of the clutch as predicted by the extrapolation was 51.8 in-lb. This value was reasonably close to the desired value and supports the validity of the design procedure that was used and the assumptions that were made.

The results from the increasing current calibration tests highlighted some key differences when compared to those obtained by Bunting with the previous system. The disk clutch configuration tested by Bunting demonstrated a torque-current sensitivity of 59.7in-lb, which is approximately 50% greater than that of the drum clutch configuration. This is apparent by the steeper linear trend for the disk clutch data. Additionally, the data obtained by Bunting seemed to demonstrate more of a linear relationship while the data for the drum clutch appeared to become increasingly non-linear as the current values approached that of the saturation current. This indicates that the saturation current of the drum clutch configuration was much closer to the highest current values that were tested during the calibration than the saturation current of the disk clutch system was to the highest current values that were tested. Thus the saturation current of the disk clutch system was higher than 1.25 Amps.

One trial exhibiting the hysteresis behavior of the drum clutch system is shown in Figure 3.3. The hysteresis effects for the drum clutch system are very similar to those for the disk clutch system obtained by Bunting (Figure 3.4) as well as another rotary MR device (Ahmadkhanlou 2005). In order to provide a straightforward comparison of data, the data labeling scheme used by Bunting was also used for the drum clutch data and is described as follows. The data represented with long dashes shows the initial holding torque of the clutch when the current is decreasing prior to the breakaway point. The line with shorter dashes represents the remaining holding torque capacity after the breakaway event occurred, as previously mentioned. A key difference in the plots for the two different systems was the degree of hysteresis observed for increasing and decreasing currents at a particular holding torque. The disk clutch system appears to exhibit 50% more hysteresis at a given holding torque than that of the drum clutch system. This increase corresponds closely to the difference in the static sensitivities of each device. The results of the static calibration will help to explain different results obtained from later experiments between the drum clutch and disk clutch systems.

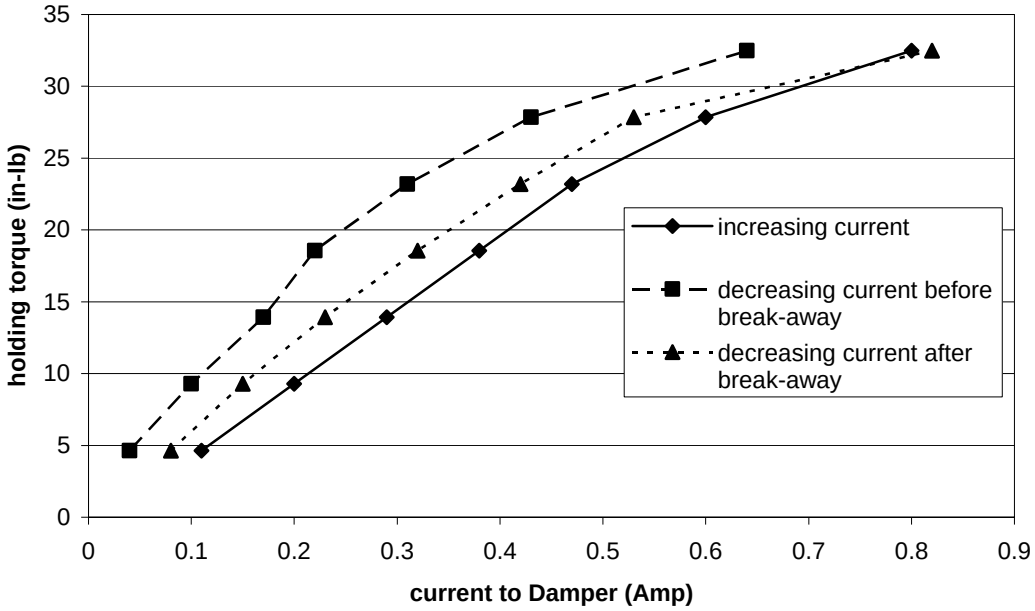

Figure 3.4: Torque-current plot demonstrating hysteresis (new system)

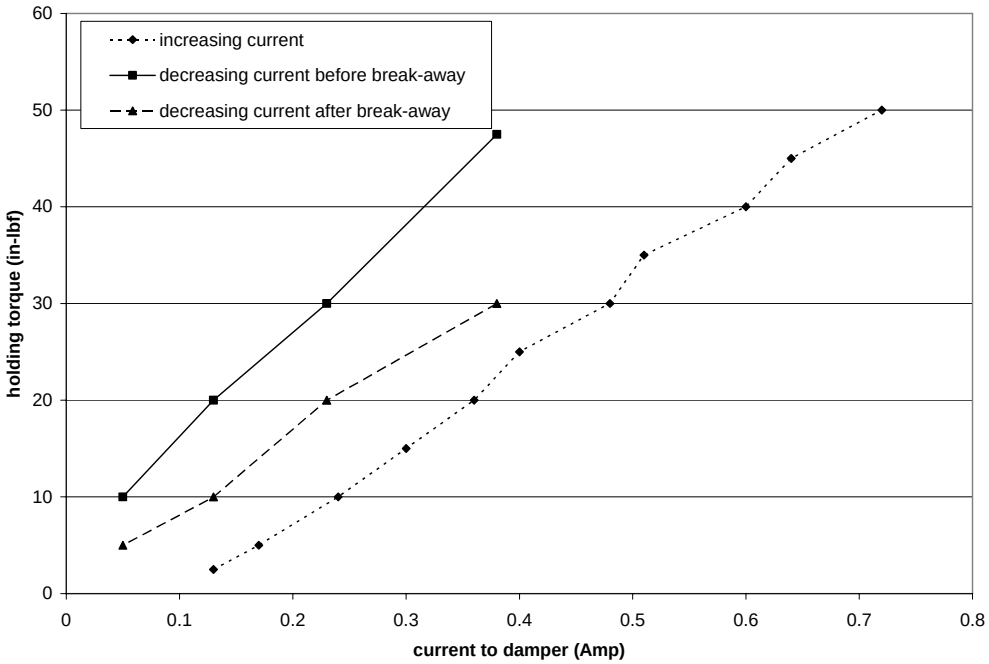

Figure 3.5: Torque-current plot demonstrating hysteresis (Bunting 2005)

3.2 Dynamic Calibration

In order to further compare the behavior of the two different systems a dynamic calibration was performed on the drum clutch. For these tests the motor was driven at a constant speed while its dynamic holding torque was observed.

The dynamic calibration was performed using the complete mechanical assembly as described in Chapter 2. The experimental set-up was similar to the one used by Bunting (2005) except that the assembly was retrofitted with the drum clutch rather than the disk clutch and a different load cell was used. The set-up is described as follows. No torsion spring was used in these tests since continuous rotation between the shaft and outer body was required. A limit switch was removed and replaced by a load cell in order to dynamically measure the forces during the calibration. The load cell was Sensotec model 31/1430-06-04 with a 100lb force limit. It was bolted to a steel block that was mounted to the polycarbonate frame in such a way as to ensure that the threaded rod extending from the body of the clutch contacted the load cell in a horizontal position with respect to the table. The distance from the axis of rotation to the point of load application was 2.5 inches. Photographs of the two different set-ups are given in Figures 3.6 and 3.7.

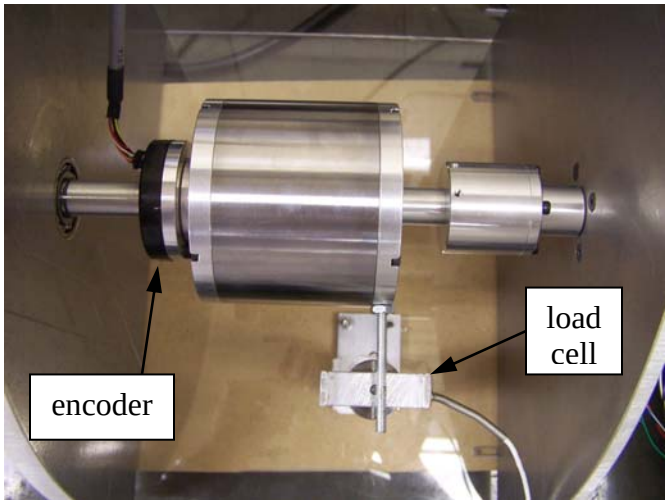

Figure 3.6: Setup for dynamic calibration (new system)

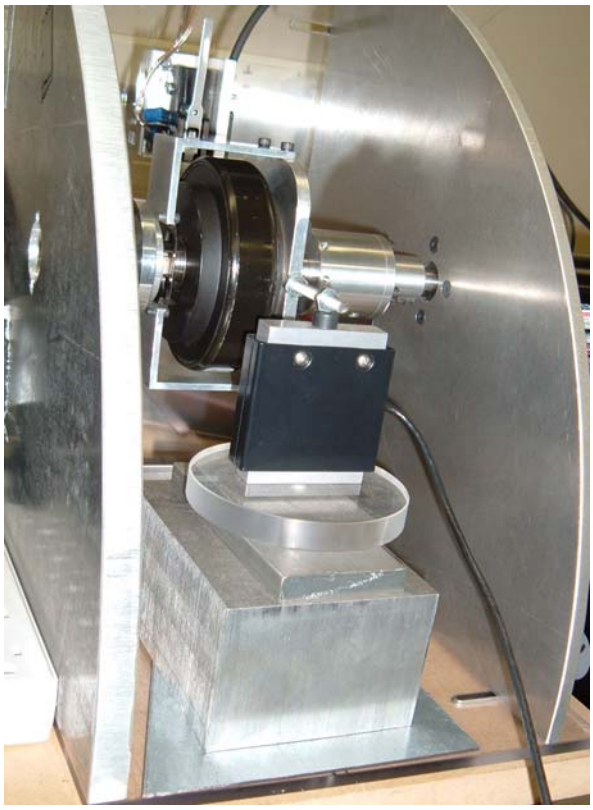

Figure 3.7: Setup for dynamic calibration (Bunting 2005)

3.2.1 Dynamic calibration test procedure

To provide a valid comparison between the drum clutch system and previous disk clutch system, Bunting's test procedure was used. A proportional-integral (PI) controller was implemented to achieve velocity control of the motor. Knowledge of the proportional and integral gains used by Bunting was not available so the gain values that were used to test the drum clutch system were obtained using the Ziegler-Nichols method. The velocity of the motor was obtained by filtering the differentiated motor encoder signal. The filter used was a low-pass with a cutoff frequency of approximately 0.8Hz. The filter was only used for post-processing purposes and was involved in the control of the mechanism. When the motor achieved the commanded angular velocity the current applied to the damper was incrementally increased in order to view the amount of torque that was resisting the motion of the motor. Both increasing and decreasing current values were used. An oscilloscope was connected to the load cell output in order with the averaging function turned 'on' in order to view a continuous output signal from the load cell. The averaged values displayed by the oscilloscope fluctuating and required visual averaging for each applied damper current. It should be noted that Bunting used a multimeter to view the load cell output because no oscilloscope was available at the time of the previous experiments. However, the use of an oscilloscope is more desirable because better measurement accuracy could be achieved.

3.2.2 Dynamic calibration test results

During the dynamic calibration experiments with the drum clutch MR rotary system, a significant oscillation in the commanded motor signal was observed. A similar phenomenon was noticed by Bunting during the experiments with the disk clutch system (see Figure 3.8). Bunting cited the source of the oscillating motor signal to be primarily caused by an apparent asymmetry due to misalignment between the damper body and the damper rotor (disk) that was fixed to the shaft (Bunting 2005, p.51). However, since no apparent asymmetry was physically observed in the drum clutch system further investigation was required to determine the cause of the oscillations in the drum clutch system.

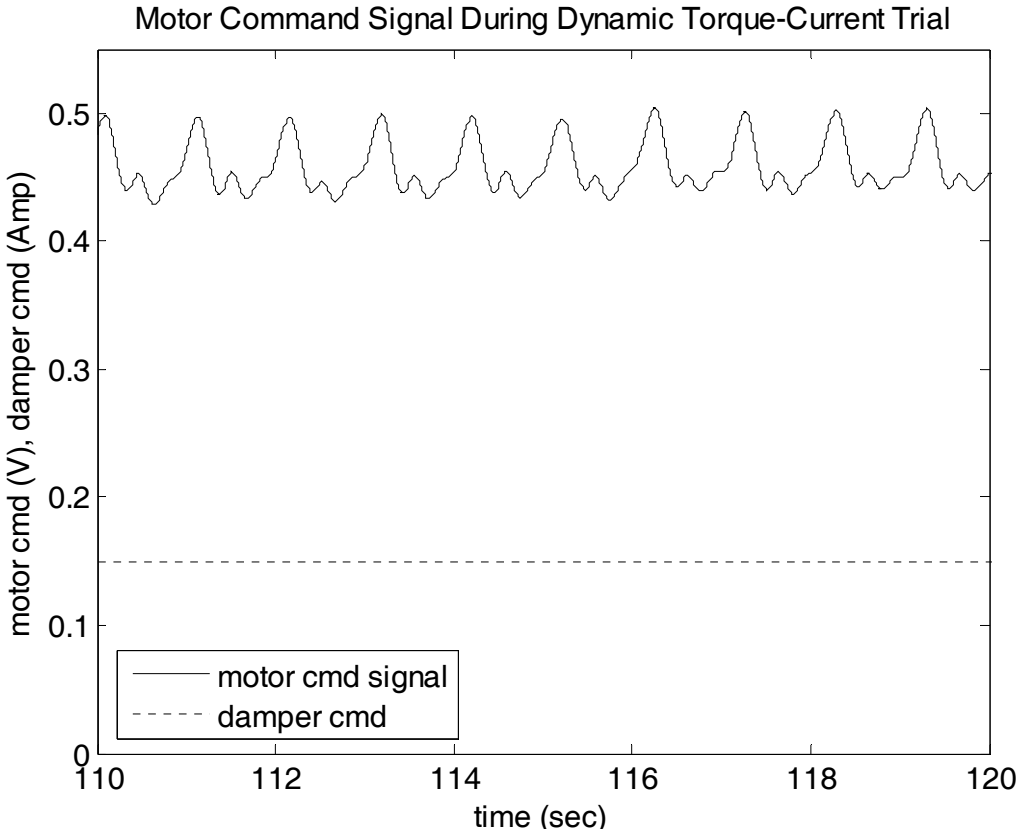

Figure 3.8: Irregular motor command signal (Bunting 2005)

In order to investigate the motor speed and applied damper current dependence of the oscillating motor command signal, motor command signals were recorded at various applied damper currents for commanded motor velocities of both 10rpm and 15rpm. These signals are displayed below in Figure 3.9. Referring only to the motor command and applied damper current signals for the 10rpm constant motor velocity, it is clear that the amplitude of the oscillations increase as the applied damper current increases. Comparing the results for the 10rpm motor velocity to the results of the 15rpm motor velocity at any specific applied damper current, it is evident that both the amplitude and frequency of the motor command oscillations increase. These results were also observed by Bunting (2005, p.52). If a significant asymmetry was in fact present in each system, such results could be expected; the damper's apparent holding torque would be greater during half of one full rotation and cause the motor control signal to fluctuate in order to maintain the desired angular velocity (Bunting 2005, p.51). Thus, the source of the motor command oscillations may or may not be caused by asymmetry in the system.

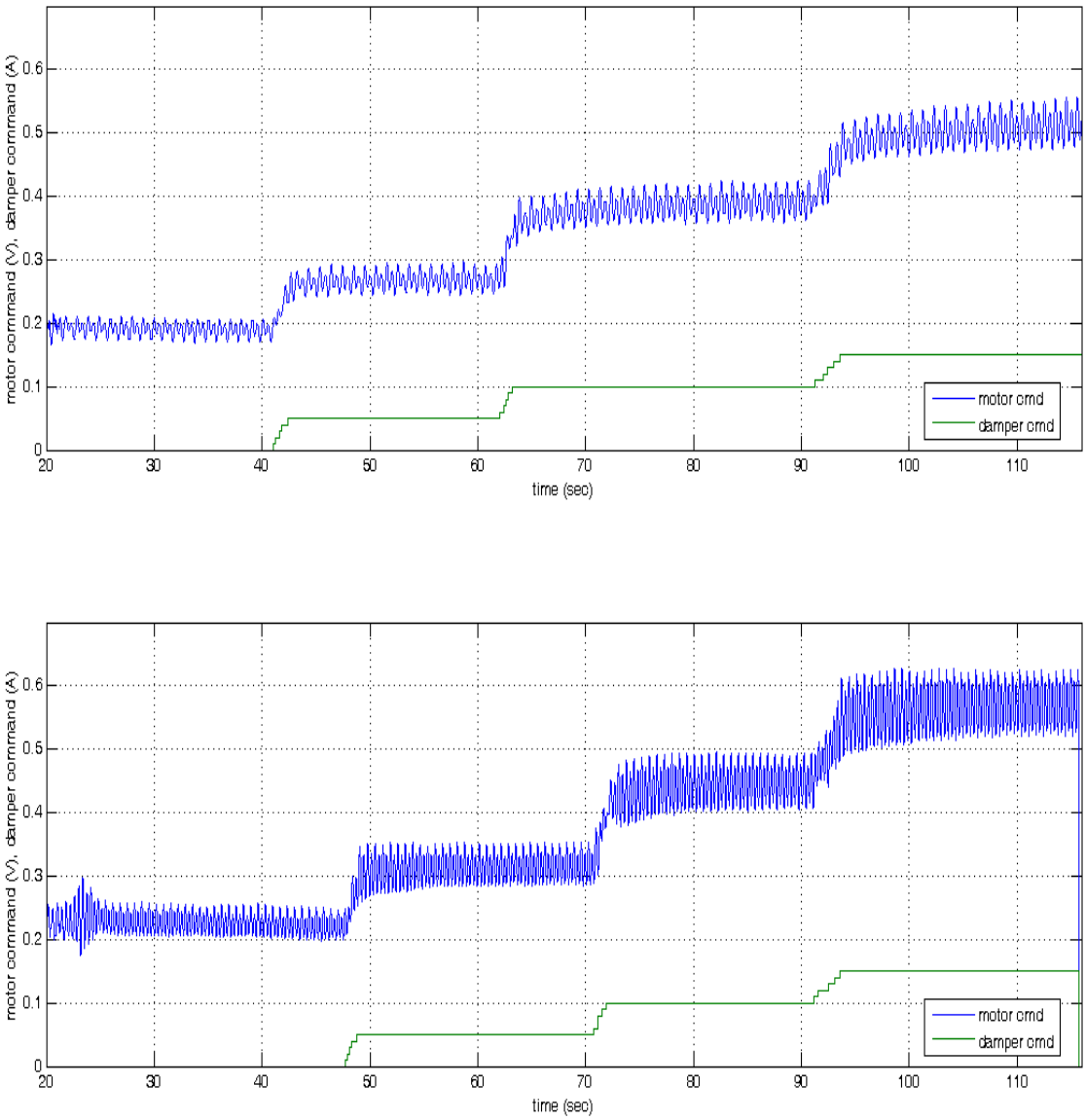

Figure 3.9: Irregular motor commands for new system (above: 10rpm motor speed, below: 15rpm motor speed)

Upon further testing of the disk clutch system it was apparent that the source of the oscillating motor command was influenced more by the nature of the controller rather than asymmetry in the system. The proportional and integral controller gains were varied

while the motor velocity and applied damper current were given constant commands. When the proportional gain was held at a constant value, the amplitude of one of the peaks in the oscillating motor command increased or decreased as the integral gain was increased or decreased. When the integral gain was held constant, the other peak in the oscillating motor command would increase and decrease as the proportional gain was increased or decreased. Since the amplitude of the oscillating motor command was significantly dependent on the choice of the controller gain values, it was concluded that the source of the oscillating motor command was largely due to the nature of the control scheme that was used during the experiments.

The chosen control scheme and resulting oscillating motor command proved to be problematic in completing the dynamic calibrations. Calibration could only be performed for relatively small motor velocities and commanded damper currents. Relatively high-applied damper currents yielded high torques that resisted the motion of the motor and caused large fluctuations in the motor command signal that were undesirable. Bunting cited similar problems in completing the dynamic calibration of the disk clutch system (Bunting 2005, p.52).

The issues with the oscillating motor command signal could be mitigated by adjusting the control scheme but was not in the interest of this research. The problems with control scheme were limited to the dynamic testing and had insignificant effects on the primary experiments.

The first three sets of data were taken at a motor speed of 10rpm using only increasing applied damper currents. The trials provided consistent results. A linear trend line was fit to the average of the three data sets and yielded a dynamic sensitivity of 35.4in-lbf/Amp. Similar tests conducted by Bunting on the disk clutch system resulted in a dynamic sensitivity of 37.3in-lbf/Amp. The results for the dynamic calibration tests of each system are presented below in Figures 3.10 and 3.11. The best-fit line in Figure 3.10 was obtained using the data shown.

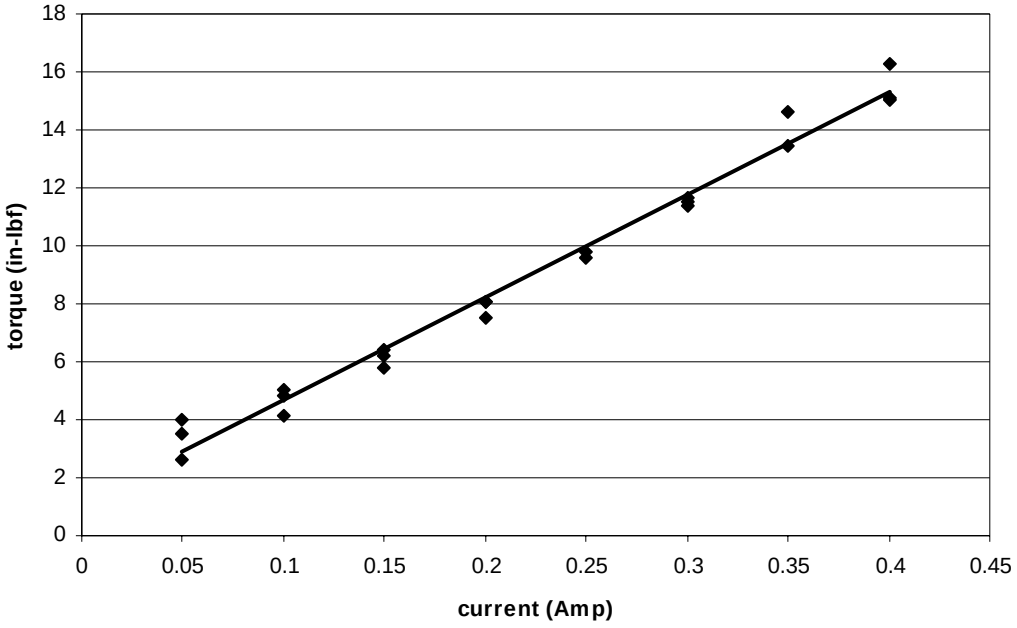

Figure 3.10: Damper torque-current data for 10rpm motor speed (new system)

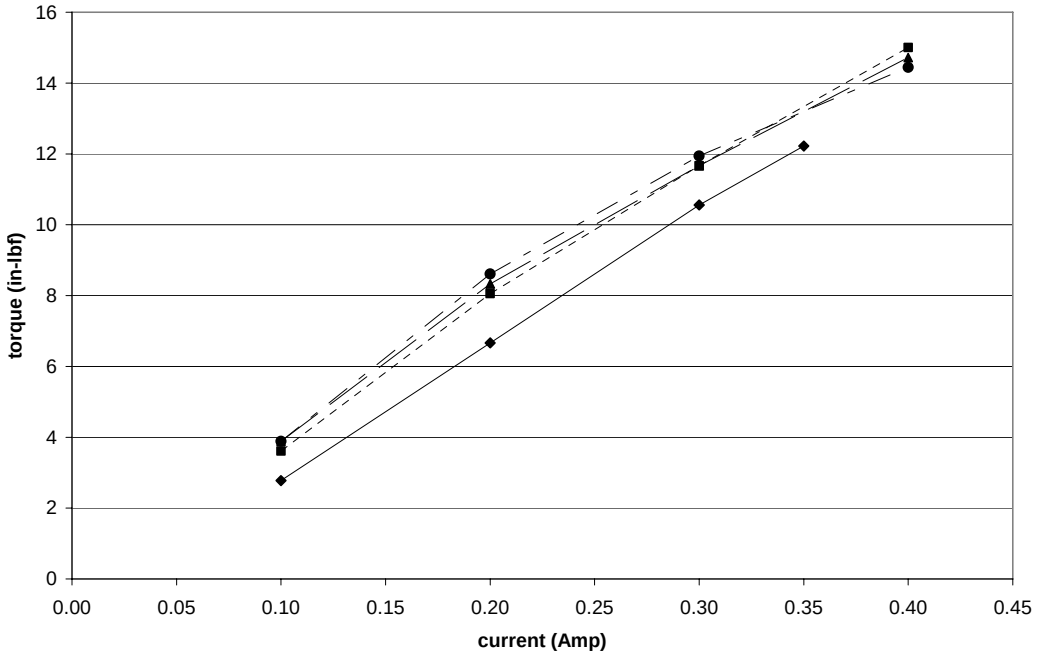

Figure 3.11: Damper torque-current data for 10rpm motor speed (Bunting 2005)

For both systems, the sensitivities decreased when comparing the static calibration results to the dynamic calibration results. However the magnitude of the decrease observed for the disk clutch system was 37% while that of the drum clutch system was only 4%. The reason for the discrepancy in the magnitude of decreased sensitivity for the two systems is not clear but could be related to a number of factors that differ between the two systems and ultimately influence the effective static and dynamic friction within the mechanisms. Some of these factors include the properties of the different magneto-rheological carrier fluids, the different methodology by which the MR fluid is contained (no foam vs. foam), etc. The fact that there exists a large discrepancy in the degree of decreased sensitivity when comparing the two systems was not pertinent to the ultimate goal of the primary testing and consequently was not investigated further.

A fourth set of data was obtained for the case of both increasing and decreasing currents while the motor was driven at a constant speed of 10rpm. The results of the test illustrate the hysteresis effects of the drum clutch system and parallel the results obtained during similar tests of other MR rotary devices such as those conducted by Bunting (2005) and An and Kwon (2003). The hysteresis effects for both the drum clutch system and disk clutch system that was tested by Bunting are apparent below in Figures 3.12 and 3.13. Bunting cited An and Kwon (2003) in explaining the hysteresis effects as a consequence of general ferromagnetic hysteresis that occurs when steel is in the presence of a magnetic field. The ferrous material present in the damper body that is required to close magnetic circuit holds its induced magnetism even after the magnetic field is taken away (Bunting 2005, p.54).

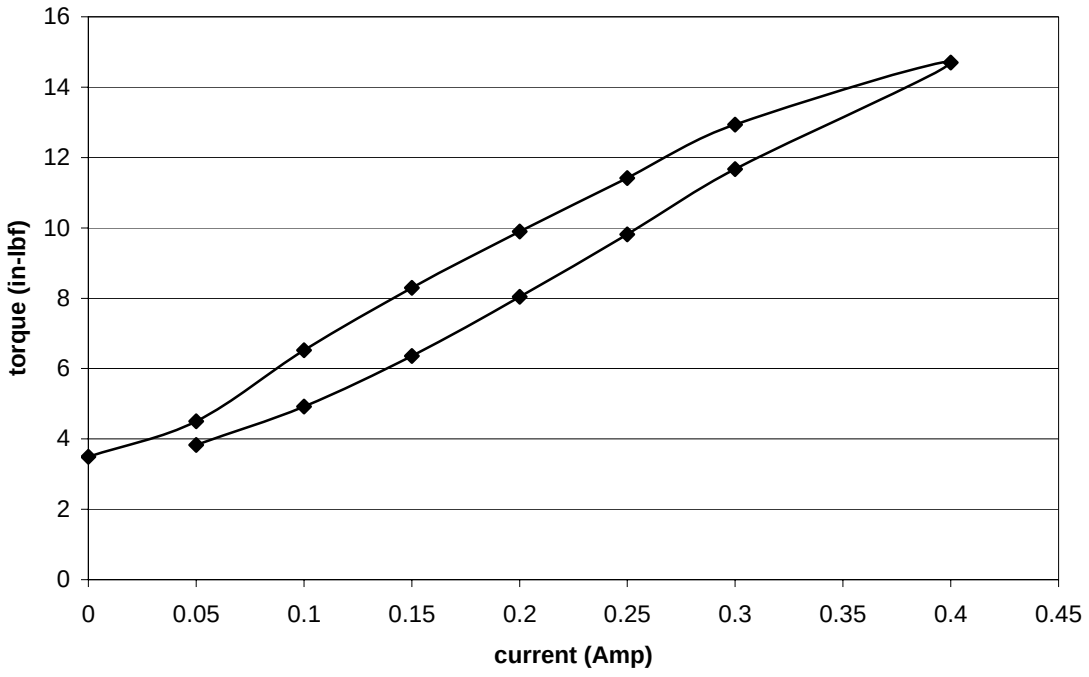

Figure 3.12: Damper hysteresis, 10rpm motor speed (new system)

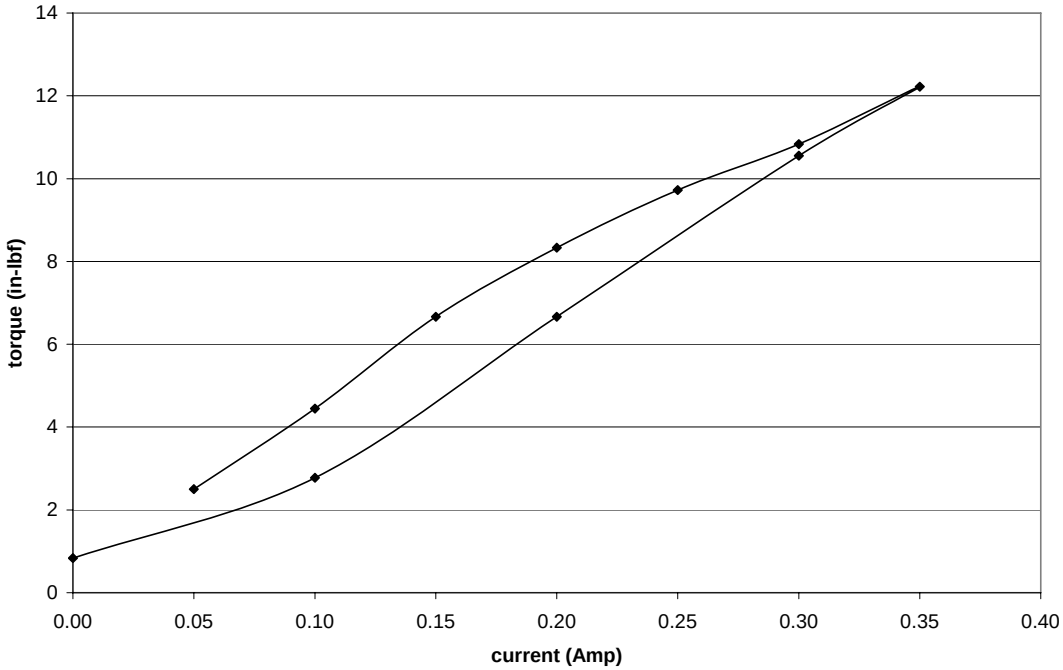

Figure 3.13: Damper hysteresis, 10 rpm motor speed (Bunting 2005)

Further testing was conducted in order to determine whether or not the drum clutch device exhibited the speed independent behavior that was observed in the disk clutch system observed by Bunting. As in Bunting,s tests, additional data was collected for 5rpm and 12rpm motor velocities. As in the disk clutch system, speed independence was displayed by the drum clutch configuration (see Figures 3.14 and 3.15).

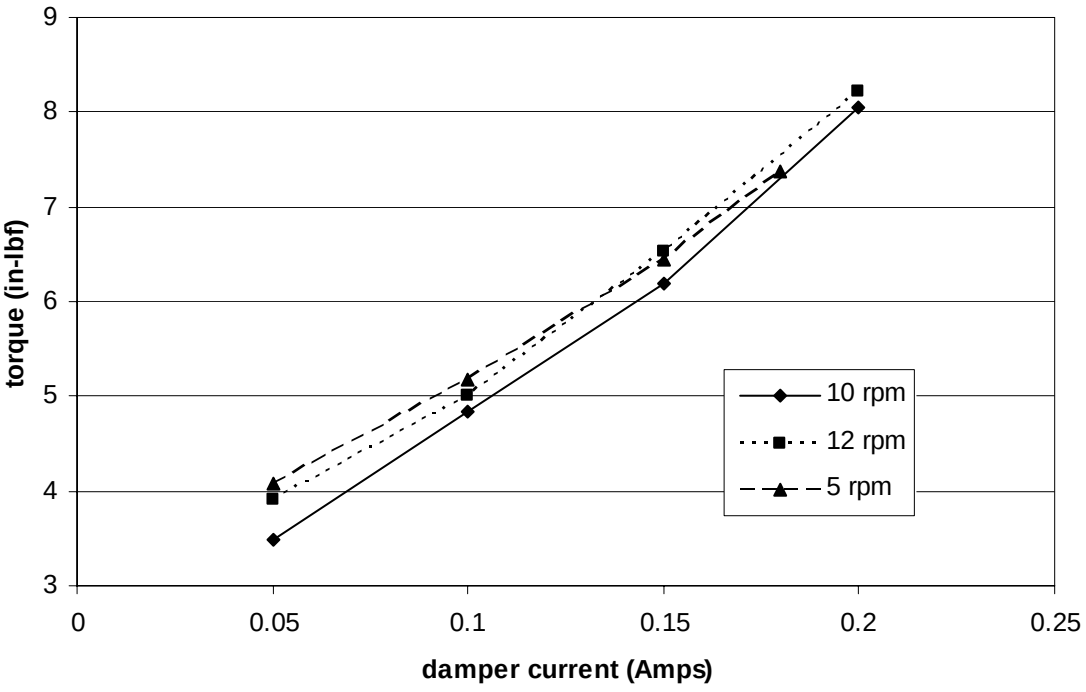

Figure 3.14: Speed independence of torque-current curves (new system)

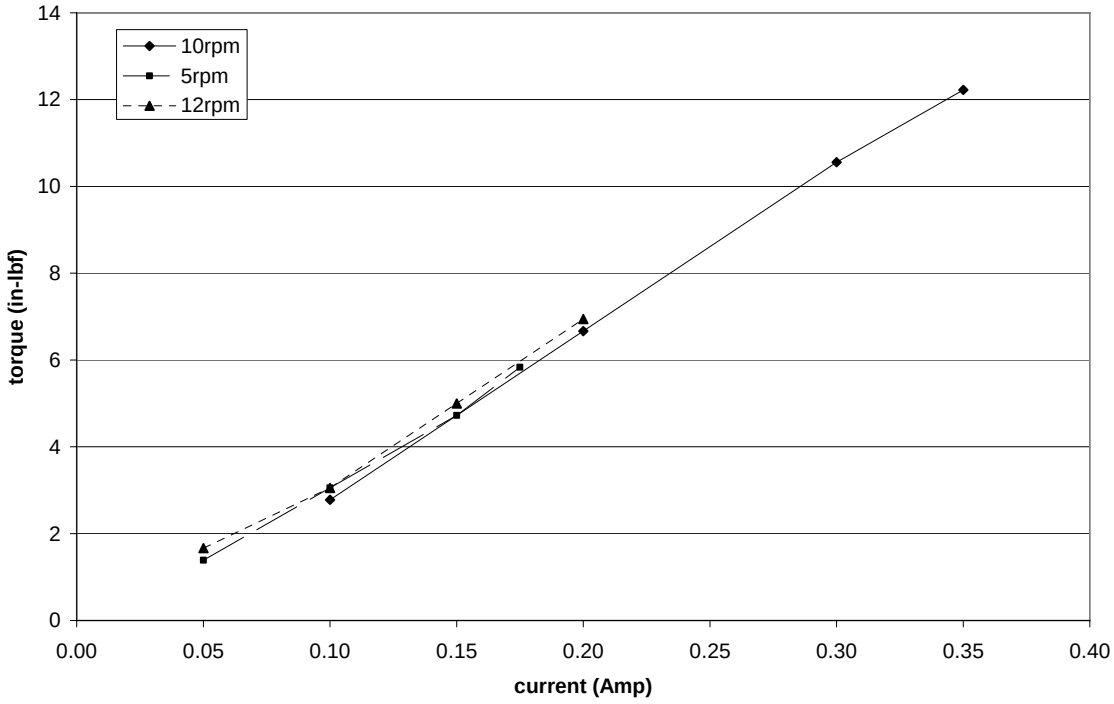

Figure 3.15: Speed independence of torque-current curves (Bunting 2005)

3.3 Control of Velocity Profile Motion with Constant Damping

The control scheme developed by Bunting in order to create a velocity profile for the disk clutch system was used for the same purpose in testing the drum clutch system. The velocity profile essentially accelerates the damper body from rest to a desired cruising velocity before decelerating it back to rest. The ultimate goal of the velocity profile testing was to optimize safety for human-manipulator interactions while maintaining precise motion. This was to be accomplished by increasing the current to the damper to realize a more rigid system at low velocities and high accelerations while decreasing the current to the damper to create a more compliant system at high velocities. Before Bunting could accomplish this with the disk clutch system, however, it was necessary to first achieve precise control by determining appropriate controller gains using constant damping (Bunting 2005, p. 56). The purpose of such testing for the disk clutch system was not to reinvent an appropriate control scheme but merely to demonstrate that the final choice of control scheme used by Bunting was appropriate for the drum clutch system. The appropriateness was based on the comparison of the observed motor error of the two systems using the same control scheme and controller gains.

The retrofitted mechanical system described in Chapter 2 was used for both the constant and variable damping experiments. The torsion spring, Century Spring model TO-5237R, was inserted back into the system and the load cell was replaced with the original limit switch. See Figure 3.16 for the complete set-up.

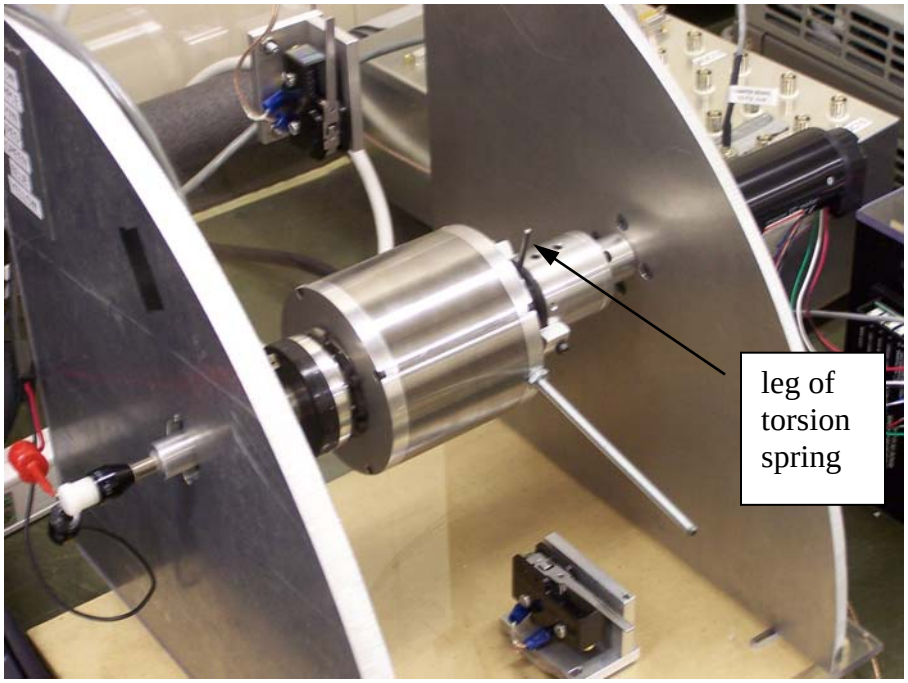

Figure 3.16: Setup for velocity profile tests

3.3.1 Control Scheme for Constant Damping Conditions

The development of Bunting's control scheme is as follows. The velocity profile was parameterized using the desired angular velocity and total rotational displacement. Inputs to the controller included initial time, t0, blend time, tb, final time, tf, initial velocity, v0, and cruising velocity, V. The initial velocity and initial time were always chosen to be zero. By intuitively choosing the blend time and final time, the rotation of the system was controlled during each phase of the profile. Bunting's final choice of parameters was: tv = 0.75sec, tf = 3.5sec, and V = 60deg/sec. These parameters corresponded to a constant magnitude of acceleration and deceleration of $80\,\mathrm{deg}/\mathrm{sec}^2$. The acceleration and deceleration phases each occurred over 22.5 degrees of travel while the constant velocity phase occurred over 120 degrees of travel, for a total rotation of 165 degrees

(Bunting 2005, p.58). The velocity profile and associated position profile created by Bunting's control scheme for the constant damping experiments are shown in Figure 3.17.

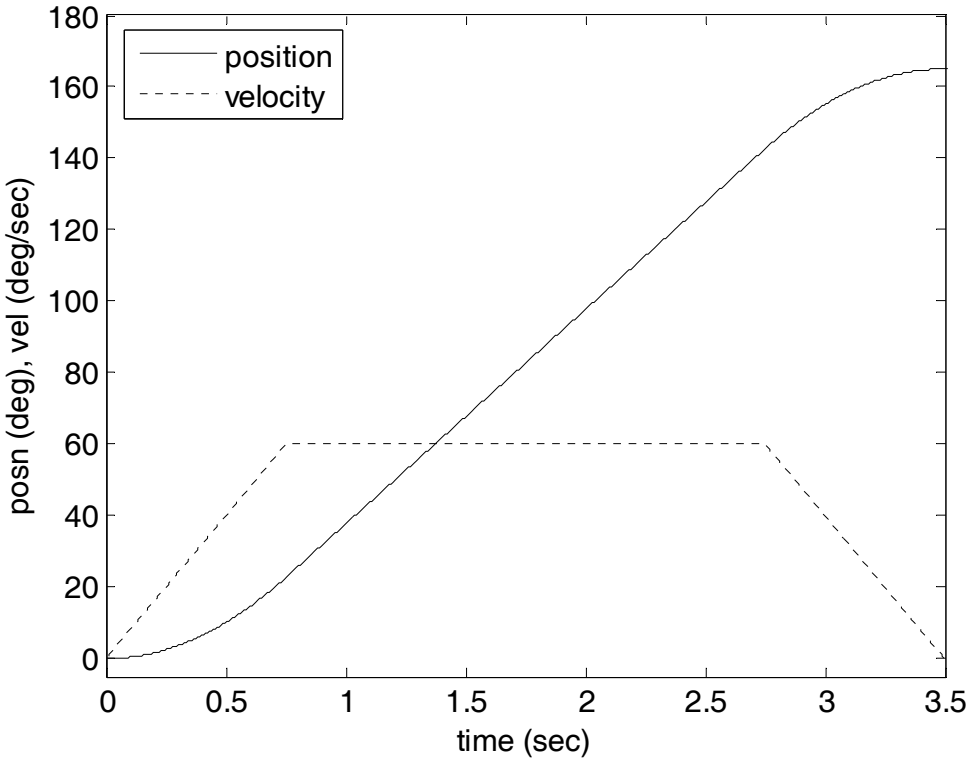

Figure 3.17: Position and velocity profiles (Bunting 2005)

3.3.2 Test Procedure for Constant Damping Conditions

The optimum controller, as determined for the disk clutch system by Bunting, was used to test the drum clutch system for constant damping conditions in order to affirm its further use in later experiments. It was only necessary to test the final set of PID gains chosen for the disk clutch system in order to compare the performance of the former system to the latter drum clutch system. If similar results were obtained, the controller

and controller gains were deemed appropriate. The optimal choice of controller gains determined for the former system were Kp = 20, Kd = 0.5, and Ki = 1.5. The previously described velocity profile and former set of optimal PID gain values were utilized in all constant-damping tests of the drum clutch system.

The threaded rod that was fixed to the damper body was placed against the limit switch mounted on the vertical polycarbonate plate. The Opal-RT model was then initiated. Next, the set of optimal gain values determined for the former system was input into the controller. The damper current was chosen to be 0.3Amps, which corresponded to the maximum current chosen for the testing of the former system during similar experiments. The velocity profile was then initiated. Pertinent data was saved to a .mat file in order to be examined and processed later using MATLAB.

3.3.3 Results from Constant Damping Experiments

The results obtained for the drum clutch system proved to be comparable to those obtained for the former disk clutch system in terms of the error (desired motor position – actual motor position) observed during the execution of the velocity profile. This supported the use of the optimum control scheme and PID controller gains obtained for the previous system to be used in further testing of the drum clutch system.

3.4 Control of Velocity Profile Motion with Variable Damping

Variable damping was utilized in the final set of velocity profile testing to verify that the MR rotary device could maintain precise control, as suggested by the results on the

previous disk clutch system, by effectively eliminating the compliance in the system introduced by the torsion spring. The results from previous tests on the disk clutch system demonstrated precise control during only the acceleration and constant cruising velocity phases of the motion. However, precision was lost during deceleration due to the backlash present in the former system. Therefore, in order to validate the concept of an MR rotary device to achieve precise control while increasing safety, it was important to repeat the velocity profile experiments using variable damping for the newly designed MR drum clutch system that contained negligible backlash.

The sets of tests that were performed on the drum clutch system were chosen to demonstrate that, as was the purpose for testing the previous system, the loss of position control occurs when no current is sent to the damper, but position control could be regained by varying the applied damper currents to create an effectively rigid system (Bunting 2005, p.64). The results of such experiments could then be compared to the suggestive but inconclusive results obtained for the disk clutch system. In order to provide a valid comparison, the spring, velocity profiles and controller gains used to test the former system were implemented during the testing of the drum clutch system. Though Bunting tested various velocity profiles and various schemes for the control of the damper current, it was only necessary to test the new drum clutch system using the final choice of damper current control scheme. Based on the previous tests that demonstrated similar responses between the two systems to the same position control scheme (section 3.3.3), it was reasonable to assume that the best control scheme for the variable damping experiments for the previous system would also work best for similar

tests of the new drum clutch system. Moreover, it did not seem necessary to test the new system with velocity profiles containing low magnitudes of acceleration since the overshoot error (amount of damper body rotation relative to the rotation of the shaft) would be maximized for profiles with high magnitudes of acceleration. Thus, the full capability of the MR rotary device to maintain precise position control could not be determined since insignificantly small currents would be required at sufficiently small accelerations.

3.4.1 Setup

During previous variable damping velocity profile experiments for the MR disk clutch rotary device, it was necessary to perform tests in both the clockwise and counterclockwise directions to demonstrate precise position control during acceleration and deceleration phases of the motion. Such bi-directional testing was required due to the backlash inherent to the previous system and the fact that acceleration caused relative displacement in one direction (i.e. winding of the spring) between the damper body and shaft while deceleration yielded relative displacement in the other direction (i.e. unwinding of the spring). By adjusting the position of the damper body with respect to the shaft prior to running experiments, one could eliminate the backlash for only one direction of motion (Bunting 2005, p.70). The new system, however, was without significant backlash (less than .025 degrees). Accordingly, the overshoot due to acceleration and deceleration of the new drum clutch system could both be examined using unidirectional testing.

The velocity profile tests that were executed using variable damping for the new drum clutch system utilized Bunting's damper current command that was created with cubic curves. The benefits of such a current command as opposed to step and ramp current commands were the continuous slope of the damper input during phase transitions (e.g. acceleration to deceleration) and the fact that the amount of motion during which the maximum current was commanded was minimized. This increases the safety because more of the motion is executed while the system is effectively compliant (Bunting 2005, Pp.70 –71). An example of a damper command with cubic curves that was created using the control scheme developed by Bunting is shown in Figure 3.17.

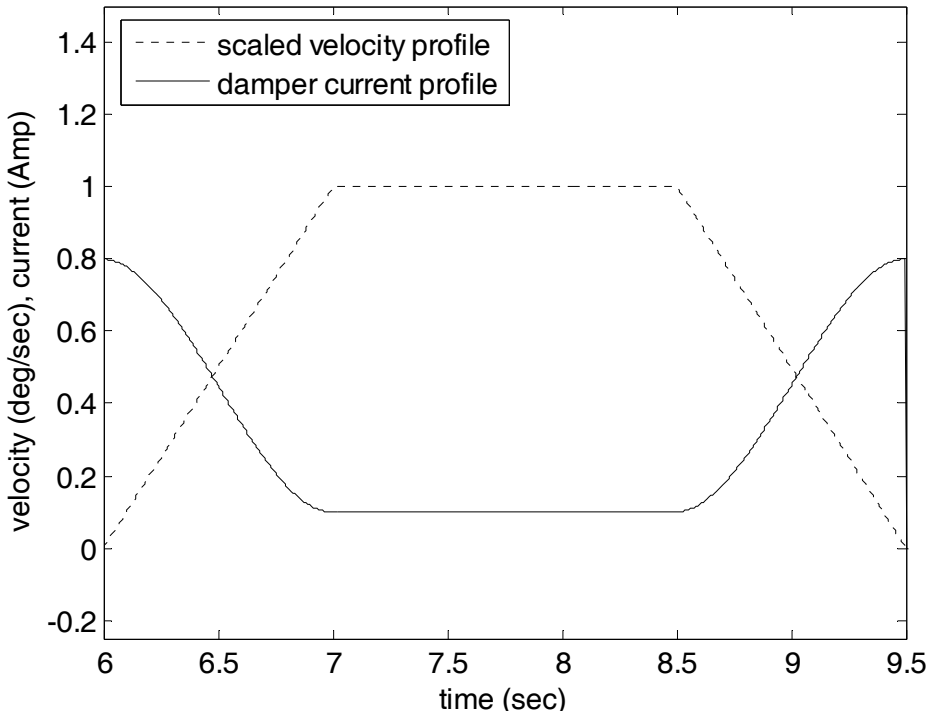

Figure 3.18: Damper current input with cubic curves

The physical set-up was same as that used during the previous constant current velocity profile tests except that torsion spring, Century Spring model TO-5230R, was placed in series between the shaft and damper body to introduce compliance into the system. The legs of the torsion spring were fixed to the damper body and bracket that was attached to the shaft by using clamps and rubber shims. The shims provided extra compression, effectively increasing the friction between the spring legs and the surfaces to which they were mounted. Fixing the spring legs with respect to the damper body and shaft served to ensure consistent results and eliminate unwanted motion of the spring.

3.4.2 Procedure for Velocity Profile Tests with Zero Applied Damper Current

To show that precision control of the MR drum clutch device was lost by introducing compliance into the system, sets of tests were completed in order to observe the amount of overshoot experienced by the system during the execution of a single velocity profile. The presence of the overshoot as a result of compliance would be undesirable in any industrial robotic system and motivated the use of the cubic current profile applied to the damper to effectively create a rigid system (Bunting 2005, p.74). The velocity profile that was used for all of the trials commanded a cruising angular velocity of 1080deg/sec and an acceleration of 7776deg/sec^2. This was the same profile that was primarily used during similar tests of the prior disk clutch device and was intentionally chosen to for the testing of the new system in order to compare results.

3.4.3 Results of the Velocity Profile Tests with Zero Applied Damper Current

The results of the tests for zero commanded damper current and the experimentally determined optimum cubic current profile are displayed in Figures 3.19 and 3.20 for both the prior disk clutch system and new drum clutch system. In each of the figures, negative values represent overshoot due to acceleration while positive values indicate overshoot due to deceleration.

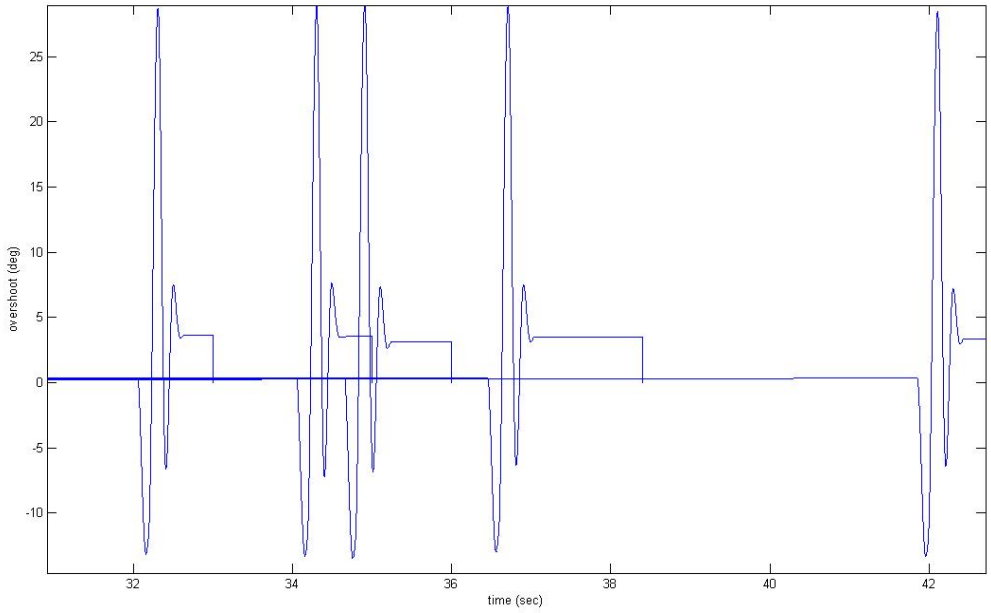

Figure 3.19: Five repeatable trials, acceleration with zero applied current (new system)

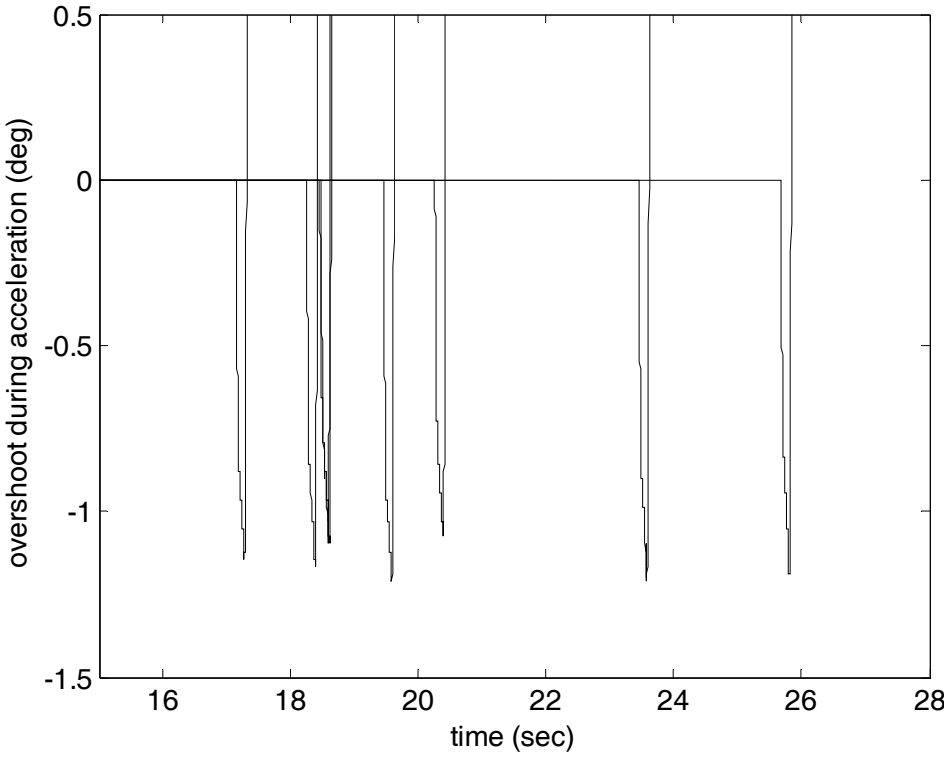

Figure 3.20: Eight repeatable trials, acceleration with zero applied current (Bunting 2005)

The figures indicate that both systems performed consistently. A key difference, though, was the discrepancy in the amount of overshoot that was observed between the two systems. The average overshoot due to the acceleration phase of the motion for the prior system was calculated to be 1.14 degrees while that of the drum clutch system was 13.5 degrees. The reason for the large discrepancy in the numbers was due to different test procedures. During the testing of the previous system, the power supply to the damper remained 'on' and a zero current was commanded to the damper. Even though zero current was commanded, a small current was still applied to the damper due to a small but significant voltage drop across the damper winding that was inherent to the electric circuit. Due to the small, applied current to the damper, some torque that resisted the

motion of the motor was present and provided additional damping during the execution of the velocity profile.

During similar tests of the new drum clutch device, the power supply to the damper was turned ‘off’ to ensure no damping effects from undesired current applied to the damper. The additional damping that was introduced to the disk clutch system because of unwanted currents was reflected by significantly smaller overshoots when compared to those experienced by the latter drum clutch system. In order to show that the discrepancy was mainly due to the phenomenon of the unwanted current, the new system was also tested with the power to the damper turned on. As expected, this yielded a comparable overshoot to that which was observed in the former system.

3.4.4 Procedure for the Velocity Profile Tests with Cubic Applied Damper Current

The ultimate goal of varying the current was to minimize the amount of current required to achieve an effectively rigid system so that safety could be maximized. In order to establish the optimum cubic current profile for a specific velocity profile, it was first necessary to use constant current commands to establish the minimum current required to achieve the desired amount of precision motion control. After this current value was determined, it was used as a starting place for establishing the maximum and minimum commanded damper current inputs for the cubic current profile (variable damping). The minimum value of the input for the cubic current profile was then incrementally decreased by 0.1 Amps until a loss of the desired degree of precise motion control was

observed. The minimum damper current was then chosen to be the one prior to the one that led to a loss of precise motion.

3.4.5 Results of the Velocity Profile Tests with Cubic Applied Damper Current

Using this methodology described above for a velocity profile with an acceleration of 7776deg/sec^2 and cruising velocity of 1080deg/sec, the optimum cubic current input to the damper had a maximum value of 0.5Amps and minimum input of 0.2Amps. The results of the variable damper currents for both systems are plotted in Figures 3.21 and 3.22, along with the results for zero applied damper current.

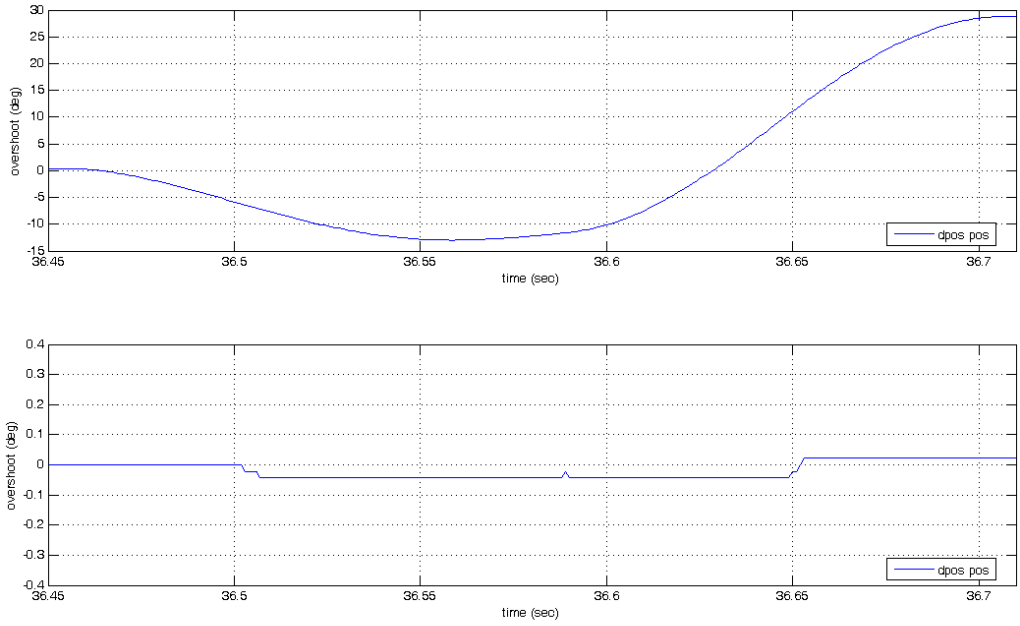

Figure 3.21: Overshoot comparison for zero current and optimum current (new system)

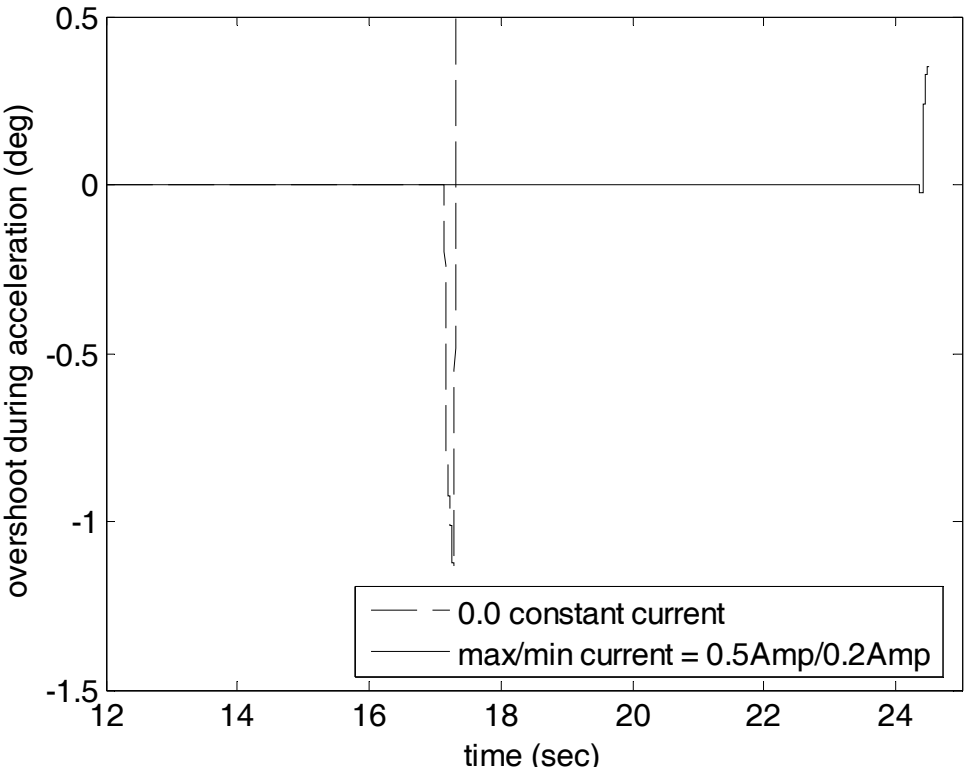

Figure 3.22: Overshoot comparison for zero current and optimum current (Bunting 2005)

The figures indicate that as was the case of the prior disk clutch system, the use of the cubic current profile for the damper produced a dramatic improvement in the degree of precision control due to acceleration as compared to the zero current case. Using the experimentally determined optimum damper profile, the overshoot experienced by the drum clutch system due to acceleration was reduced to .04 degrees. Using the same current profile, the previous disk clutch system exhibited approximately .02 degrees of overshoot during acceleration. Again, the overshoot due to acceleration caused winding of the spring and is represented in the figure by negative overshoot values. The overshoot due to deceleration, however, could not be compared due to the backlash in the previous system.

The evidence of the backlash present in the previous disk clutch system was reflected in the above figure and proved to be problematic in comparing the overshoot of the damper body with respect to the shaft. Because of the overshoot in the previous disk clutch system, the resistive torque provided by the damper could not be effectively applied in both directions until the approximately two degrees of backlash was taken up by the rotation of the damper body. Overshoot values caused by the deceleration of the systems were represented by positive values of overshoot (unwinding of the spring). The actual amount of overshoot due to deceleration for the previous disk clutch system after the initial acceleration and cruising velocity phases is shown to be approximately 0.35 degrees, which is significantly higher than the corresponding plot for the new drum clutch system. By comparing the plots for the two systems for the case of variable damping, it was clear that the drum clutch system effectively mitigated overshoot due to deceleration while the previous drum clutch system did not.

3.5 Impact Testing

After demonstrating that the new MR drum clutch rotary device could conclusively maintain precision motion control using varied applied damper currents, impact tests were conducted and compared to the results to those previously obtained by Bunting using an MR disk clutch. The primary purpose in creating the effectively variable compliance transmission was to introduce series compliance to increase safety without compromising position control (Bunting 2005, p.80). During the impact testing the compliance within the MR rotary system was exploited to reduce impact forces and ultimately increase safety.

3.5.1 Impact Test Setup

The mechanical setup for the impact tests was exactly the same as that of the velocity profile tests described earlier, except that torsion spring TO-5230R was placed in series between the shaft of the clutch and the damper body. The threaded rod that served as the end-effector contacted the load cell at an average distance of 3.0 inches from the axis of rotation of the mechanism's shaft. This set-up mirrored the setup used by Bunting to test the previous system with the obvious exception being the retro-fitting of the new drum clutch as opposed the disk clutch.

3.5.2 Impact Test Procedure

The control scheme developed for the impact tests performed with the previous disk clutch system was employed to conduct impact tests on the new drum clutch system. Each trial would begin with the end-effector oriented vertically downward. In all trials, the current to the damper was held at a constant to eliminate hysteresis effects. After initiating the controller, the motor would start from rest and accelerate to a cruising velocity over 45 degrees of travel. The cruising velocity was then maintained for another 225 degrees of travel before impacting the load cell. Upon impact, the controller was manually stopped using the on-screen 'pause' button. Data from the impact was collected using an oscilloscope that was set to automatically trigger by defining an 'edge' condition. After being triggered, the scope would obtain data over a short time period that was determined by the chosen resolution of the time scale. Data from the impact was then saved on a floppy disk in 'comma separated variable' format.

The cruising velocities and applied damper currents that were tested corresponded to those chosen for the testing the previous disk clutch system in order to more easily compare results. The device was tested at cruising velocities of 15rpm, 20rpm, 25rpm, 30rpm, 35rpm, and 50rpm. For each velocity, individual tests were performed at commanded damper currents of 0Amps, 0.2Amps, 0.4Amps, 0.6Amps, 0.8Amps, and 1.0Amps. Three trials were performed at each commanded damper current and motor cruising velocity in order to check for repeatability.

3.5.3 Impact Test Results

The results of the Impact tests are presented in Figure 3.22, as well as those obtained from testing performed on the previous disk clutch system (Figure 3.24). The individual data points in Figure 3.23 represent an average from the three trials that were performed at specific speed for a specific current. Also, the percentage of impact load reduction for the case of 1.0 Amps of applied damper current as compared to zero applied damper current are tabulated below for both the disk clutch system and drum clutch system (see Tables 3.1 and 3.2).

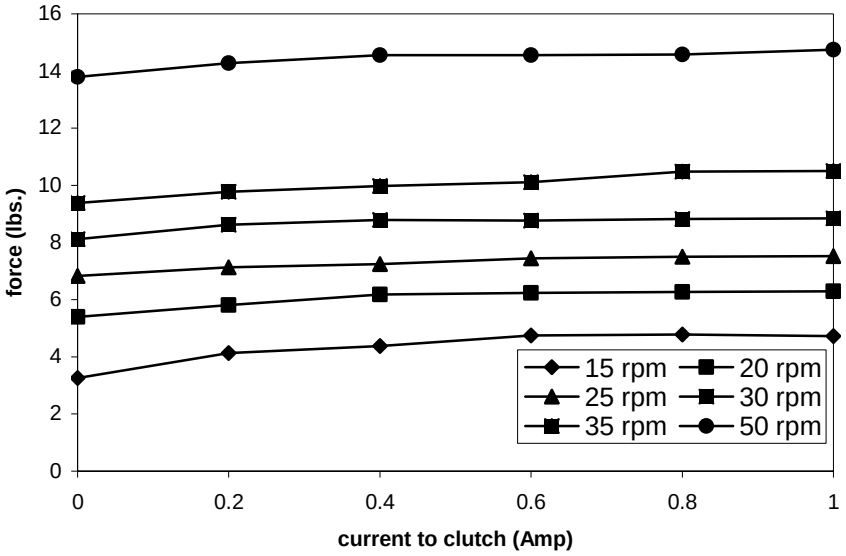

Figure 3.22: Comparison of impact forces for varying cruising velocities (new system)

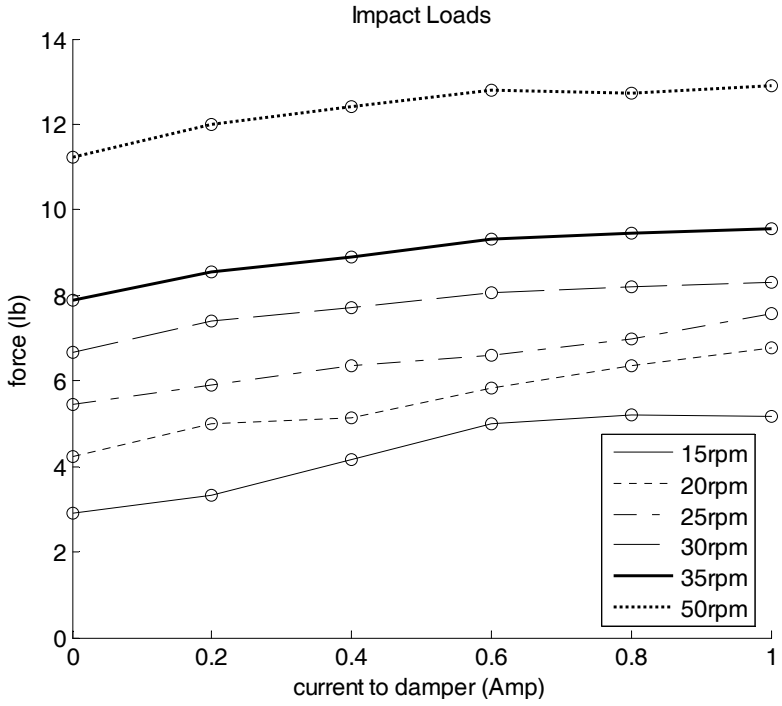

Figure 3.23: Comparison of impact forces for varying cruising velocities (Bunting 2005)

Table 3.1: Percent reduction in impact loads for various cruising velocities (new system)

speed (rpm)	15	20	25	30	35	50
% reduction of impact load	32.0	14.0	9.0	8.0	11.0	6.0

Table 3.2: Percent reduction in impact loads for various cruising velocities (Bunting 2005)

speed (rpm)	15	20	25	30	35	50
% reduction of impact load	43.4	37.5	28.1	19.8	17.4	12.9

As was the case for the previous system, the drum clutch device exhibited expected trends. Impact loads increased as the cruising velocity at impact increased for any specific applied damper current value. Additionally, impact loads increased as the applied damper current increased for any specific cruising velocity. A key difference was that the previous system displayed a larger (43.4%) percent reduction of impact as compared to the new system (32.0%). One reason for the discrepancy was most likely due to the higher static sensitivity of the previous system as compared to the new. Therefore, at a specific speed the range of the effective holding torque for the new system was smaller than that of the prior. Also the motor-side inertia of the new system was estimated to be 25% higher than that of the previous. So, the amount of the inertia that the new system attempted to uncouple from the end-effector was larger, thus yielding higher impact loads and less of a safety benefit.

CHAPTER 4: CONCLUSIONS

The primary goal of this project was to compliment testing of a prototype variable effective compliance transmission that incorporated an MR rotary device, especially by demonstrating precise position control while executing trajectories with high magnitude acceleration and deceleration phases. A new system was designed and built that was free of backlash that proved to be problematic in attaining desirable results with the previous system. Similar tests and procedures were used for the new system in order to compare results to those of the former system. By comparing the results, important similarities and differences between the systems could be highlighted and identified for further investigation.

4.1 Summary of Results

A new MR rotary device was designed and built based on the specifications of the previous device. The new device was to provide a holding torque of approximately 50in-lb. The length of the outer casing was 3.065 inches and the diameter was 3.36 inches. The length of the shaft was 8.5 inches. In order to retrofit the new device into the previous mechanical apparatus, the poly-carbonate plates that served as the frames of the old system had to be replaced with frames that were approximately 2.5 inches longer. The inertia of the new MR device on the end-effector side was approximately 90% of that

for the previous system. The inertia on the motor side for the new MR device was calculated to be 25% larger than that of the original prototype.

Static and dynamic calibrations were performed to characterize the new MR rotary device. The static sensitivity of the new MR system was 41.4in-lbf per 1.0Amp as compared to 59.7in-lbf per 1.0Amp of the previous system. At the saturation current of 1.25Amps for the new system, the holding torque was estimated to be 51.8in-lbf based on an extrapolation using the experimentally determined static sensitivity. This is close to the holding torque of 50in-lbf, which the device was designed to provide. The dynamic calibrations for the new system yielded a dynamic sensitivity of 35.4in-lb/Amp as compared to the 37.3in-lbf/Amp of the previous system. As was the case for the previous MR disk system, the new MR drum system exhibited hysteresis and speed independence during the calibration tests. The dynamic calibration tests also yielded the undesired oscillating motor commands that were first noticed in the original prototype. Further investigation into the issue showed that the source of the oscillations was mostly due to the nature of the controller rather than a mechanical issue such as asymmetry.

Velocity profile testing for constant currents was conducted to show that the control scheme developed for the original prototype was tenable for the new MR rotary system. Similar motor errors were exhibited by the new system, as compared to those observed for the previous system when the same velocity profile, damper current, and PID gains were implemented. Thus, the control scheme used for the previous system was also valid for the new system.

Velocity profile testing with variable damping was conducted to demonstrate the improved position control of the new system that lacked backlash, as compared to the previous system that contained significant backlash. Only a single velocity profile was used. It was chosen because of the high magnitude of the acceleration and deceleration (7776deg/sec^2), which would exploit the capabilities of the MR damper to achieve precise positioning versus a similar system with backlash. The new system was able to limit overshoot error to 0.04% throughout the entire velocity profile while the previous system could only show such precision during certain phases.

Finally, impact tests were conducted to investigate the potential safety benefits of the new system as compared to the prior. Impact forces were obtained at five different cruising velocities and various applied damper currents. Some general parallels were noticed between the results for the new system versus the previous system. Both configurations exhibited increased transmitted impact forces as cruising velocity and damper currents increased. The prior system demonstrated a maximum of 43.4% reduction of impact load due to varying the damper current. The new system displayed a maximum of 32.0% reduction of impact load. The difference in the static sensitivities and the end-effector side inertias were identified as the probable cause of the variance in the percent reduction of impact load displayed by the two systems.

4.2 General Conclusions

There are a number of conclusions that can be drawn from the results of the aforementioned tests. First, the performance of the new system was comparable to that of the prior, demonstrating valid design techniques and good quality construction. Accordingly, such techniques could be employed to develop new systems. Secondly, the new system was able to demonstrate precise motion control throughout an entire velocity profile. This provided essential decisive evidence that complimented research conducted by Bunting (2005) with a prior prototype that was inhibited due to backlash that was inherent to the design. Though not to the same extent as the prototype, the new system demonstrated improved safety by increasing the applied damper current, thus yielding smaller impact loads. The results support further research to develop a system that could be practically implemented in an industrial manipulator to realize the safety benefits as outlined by Bicchi and Tonietti (2004).

4.3 Future Work

Practical implementation into a pedal robot or industrial manipulator is hindered due to various factors present in the current designs. Minimizing inertia and size while increasing the range of the holding torque of an MR device should be the primary focus of future work. This would require a more refined design procedure that could be used to optimize designs for specific factors. Hysteresis could also prove to be problematic to practical implementation. It is therefore necessary to investigate ways to minimize hysteresis effects without sacrificing the system's performance. Developing a control scheme that accounts for hysteresis would also be necessary for practical applications.

Various MR device configurations (e.g. disk, drum, etc.) should be tested in order to draw further comparisons and optimization of the factors described above.

APPENDICES

Appendix A

The following script was used to automate the design procedure for the MR drum rotary device.

```
%MR DRUM CLUTCH DESIGN
%KYLE M. SABATKA

clear;clc

%THIS CODE AIDS IN THE MECHANICAL AND MAGNETIC CIRCUIT
DESIGN OF AN MR DRUM CLUTCH.  THE MECHANICAL PORTION
DETERMINES EITHER THE RADIUS OR LENGTH OF THE DRUM FOR A
CERTAIN MR FLUID AND DESIRED ON-STATE TORQUE.  THE MAGNETIC
CIRCUIT PORTION OUTPUTS EITHER THE REQUIRED NUMBER OF TURNS
OR NECESSARY CURRENT FOR A GIVEN GEOMETRY AND MR FLUID.

%%%%%%%%%%%%%%%%%%%%%%%%%%%%%%%%%%%%%%%%%%%%%%%%%%%%%%%%%%%%%%%%%%%%%%%
%%%%%%%%%%%%%%%%%%%%%%%%%%%%%%%%%%%%%%%%%%%%%%%%%%%%%%%%%%%%%%%%%%%%%%%

%MECHANICAL DESIGN



%%%%%%%%%%%%%%%%%%%%%%%%%%%%%%%%%%%%%%%%%%%%%%%%%%%%%%%%%%%%%%%%%%%%%%%
%INPUTS
%%%%%%%%%%%%%%%%%%%%%%%%%%%%%%%%%%%%%%%%%%%%%%%%%%%%%%%%%%%%%%%%%%%%%%%
%INPUT THE DESIRED ON-STATE TORQUE IN (N-m) AND SAFETY
FACTOR

T=5.61          %(N-m)
FS=1.0000

%CHOOSE AN MR FLUID AND INPUT THE MAX YIELD STRESS (kPa)
SHOWN ON THE "YIELD STRESS VS. MAGNETIC INDUCTION" PLOT

tau=40        %(kPa)
```

```
%IF YOU ARE DESIGNING FOR THE RADIUS OF THE DRUM GIVEN A
DESIRED LENGTH,
%INPUT THE LENGTH (cm) FOR 'L' AND INPUT A '0' FOR 'R'.  IF
YOU ARE
%DESIGNING FOR THE LENGTH OF THE DRUM GIVEN A DESIRED
RADIUS,INPUT THE RADIUS (cm) FOR 'R' AND A '0' FOR 'L'.


L_cm=0          %(cm)

R_cm=3.4925     %(cm)

%%%%%%%%%%%%%%%%%%%%%%%%%%%%%%%%%%%%%%%%%%%%%%%%%%%%%%%%%%%%%%%%%%%%%%%%
%MECHANICAL CALCULATIONS
%%%%%%%%%%%%%%%%%%%%%%%%%%%%%%%%%%%%%%%%%%%%%%%%%%%%%%%%%%%%%%%%%%%%%%%%

T=FS*T         %APPLIES THE SAFETY FACTOR
if R_cm==0
    R_cm=abs(sqrt((T/(4*pi*tau*10*L_cm))))*100
    L_cm
    total_L_cm=4*L_cm
    R_inch=R_cm/2.54
    L_inch=L_cm/2.54
    total_L_inch=4*L_inch
end
if L_cm==0
    R_cm
    L_cm=(T*100)/(4*pi*tau*R_cm^2*.1)
    total_L_cm=4*L_cm
    R_inch=R_cm/2.54
    L_inch=L_cm/2.54
    total_L_inch=4*L_inch
end

%%%%%%%%%%%%%%%%%%%%%%%%%%%%%%%%%%%%%%%%%%%%%%%%%%%%%%%%%%%%%%%%%%%%%%%%
%%%%%%%%%%%%%%%%%%%%%%%%%%%%%%%%%%%%%%%%%%%%%%%%%%%%%%%%%%%%%%%%%%%%%%%%

%MAGNETIC CIRCUIT DESIGN

%%%%%%%%%%%%%%%%%%%%%%%%%%%%%%%%%%%%%%%%%%%%%%%%%%%%%%%%%%%%%%%%%%%%%%%%
%%%%%%%%%%%%%%%%%%%%%%%%%
%INPUTS
%%%%%%%%%%%%%%%%%%%%%%%%%%%%%%%%%%%%%%%%%%%%%%%%%%%%%%%%%%%%%%%%%%%%%%%%

%LOCATE THE VALUE OF THE MAGNETIC INDUCTION REQUIRED TO
ACHIEVE THE MAXIMUM
```

```
%YIELD STRESS OF THE CHOSEN MR FLUID ON THE "YIELD STRESS
VS. MAGNETIC
%INDUCTION" PLOT.  USE THIS VALUE TO DETERMINE THE
CORRESPONDING MAGNETIC FLUX
%DENSITY (TESLA) THROUGH THE MR FLUID BY EXAMINING THE
"MAGNETIC FLUX DENSITY
%VS. MAGNETIC INDUCTION" PLOT.  INPUT THE DETERMINED VALUE
OF THE MAGNETIC
%FLUX DENSITY (TESLA).

B= 1.0          %(T)

%INPUT THE SHAFT DIAMETER (cm)

dia= 1.5875       %(cm)

%INPUT THE THICKNESS OF THE MR SOAKED FOAM (mm)

tf=3.1          %(mm)

%INPUT THE THICKNESS OF THE OUTER STEEL CASING (mm)

tc= 4.7625        %(mm)

%INPUT THE MAXIMUM AVAILABLE CURRENT (E.G. FROM CURRENT
SOURCE)

I=1         %(A)

%%%%%%%%%%%%%%%%%%%%%%%%%%%%%%%%%%%%%%%%%%%%%%%%%%%%%%%%%%%%%%%%%%%%%%%%%%%%
%CONSTANTS
%%%%%%%%%%%%%%%%%%%%%%%%%%%%%%%%%%%%%%%%%%%%%%%%%%%%%%%%%%%%%%%%%%%%%%%%%%%%

%PERMEABILITY VALUES

Mu0=4*pi*10^(-7);       %(H/m)
MuSteel=2000*Mu0;       %(H/m)
MuMR=3.5*Mu0            %(H/m)

%COPPER WIRE GAGE DIAMETERS (inches) ACCORDING TO A.W.G.

AWG_24= 0.022           %(in.)
AWG_26= 0.018           %(in.)
AWG_28= 0.014           %(in.)
AWG_30= 0.012           %(in.)
```

```
%%%%%%%%%%%%%%%%%%%%%%%%%%%%%%%%%%%%%%%%%%%%%%%%%%%%%%%%%%%%%%%%%%%%%%%
%MAGNETIC CIRCUIT CALCULATIONS
%%%%%%%%%%%%%%%%%%%%%%%%%%%%%%%%%%%%%%%%%%%%%%%%%%%%%%%%%%%%%%%%%%%%%%%

%CONVERSION TO SI UNITS

dia=dia/100;
tf=tf/1000;
tc=tc/1000;
R=R_cm/100;
L=L_cm/100;
H=R-dia/2;
h=H/3;

%DETERMINE THE RELUCTANCE IN EACH OF THE SIX REGIONS IN THE
MR DRUM CLUTCH

%REGION 1

L1=2.5*h
R1_avg=(dia/2)+1.75*h
alpha1=L
A1=2*pi*R1_avg*alpha1
Mu1=MuSteel
Rel1=L1/(Mu1*A1)

%REGION 2

L2=tf
R2_avg=R+tf/2
alpha2=L
A2=2*pi*R2_avg*alpha2
Mu2=MuMR
Rel2=L2/(Mu2*A2)

%REGION 3

%PART a
L3a=tc/2
R3a_avg=R+tf+tc/2
alpha3a=L
A3a=2*pi*R3a_avg*alpha3a
Mu3a=MuSteel
Rel3a=L3a/(Mu3a*A3a)
```

```
%PART b
L3b=3*L
A3b=pi*((R+tf+tc)^2-(R+tf)^2)
Mu3b=MuSteel
Rel3b=L3b/(Mu3b*A3b)

Rel3c=Rel3a         %EQUIVALENT REGIONS

Rel3=Rel3a+Rel3b+Rel3c

%REGION 4

Rel4=Rel2           %EQUIVALENT REGIONS

%REGION 5

Rel5=Rel1           %EQUIVALENT REGIONS

%REGION 6

L6=3*L
A6=pi*((dia/2+h)^2-(dia/2)^2)
Mu6=MuSteel
Rel6=L6/(Mu6*A6)

%SUM RELUCTANCE FROM EACH REGION

Rel=Rel1+Rel2+Rel3+Rel4+Rel5+Rel6   %(A/Wb)

%DETERMINES THE MAGNETIC FLUX THROUGH THE MR FLUID.  SINCE
THE MAGNETIC FLUX
%DENSITY THROUGH THE MR FLUID AND THE AREA OF THE MR FLUID
ARE BOTH KNOWN,
%THE MAGNETIC FLUX THROUGH THE MR FLUID CAN BE CALCULATED.
THE MAGNETIC
%FLUX THROUGH THE ENTIRE MAGNETIC CIRCUIT IS CONSTANT, THE
FLUX THROUGH THE
%THE MR FLUID IS EQUIVALENT TO THE FLUX THROUGH THE ENTIRE
MAGNETIC
%CIRCUIT.

A_MR=A2;
Flux=B*A_MR     %(Webers)
```

```
%DETERMINES THE MINIMUM NUMBER OF TURNS REQUIRED TO ACHIEVE
THE DESIRED
%MAXIMUM TORQUE ASSUMING MAXIMUM AVAILABLE CURRENT.

N_min=Flux*Rel/I    %(# OF TURNS)

%DETEMINES THE THEORETICAL NUMBER OF TURNS THAT CAN
ACTUALLY BE WOUND ABOUT
%THE MR DRUM CLUTCH FOR VARIOUS WIRE GAUGES.

N_24=0.75*(4*h*L)/((pi*(AWG_24*.0254)^2)/4)
N_26=0.75*(4*h*L)/((pi*(AWG_26*.0254)^2)/4)
N_28=0.75*(4*h*L)/((pi*(AWG_28*.0254)^2)/4)
N_30=0.75*(4*h*L)/((pi*(AWG_30*.0254)^2)/4)
```

Appendix B

The inertia values of the system are included in the table A.1 below. The cells that are highlighted with '**' contain values that were calculated by hand for the new system (see below). All other inertia values were obtained from Bunting (2005).

$1\text{lbm-in}^2 = 2926.55\text{g-cm}^2$

Table B.1: Inertia values for new system

gearhead	15.0
spool + copper	5303.0 **
coupling (gearhead side)	41.0
coupling (damper side)	190.2
TOTAL, motor side	**24759.2**
damper rotor	400.4
damper MR fluid	891.0
damper encoder	292.5
end-effector rod	1497.9
damper housing	10798.0 **
TOTAL, end-effector side	**13879.8**

Table B.2: Inertia values for previous system (Bunting 2005)

	value (g-cm^2)
motor, actual	85.0
motor, reflected	19125.0
gearhead	15.0
damper shaft	83.4
coupling (gearhead side)	41.0
coupling (damper side)	190.2
TOTAL, motor side	**19454.6**
damper rotor	400.4
damper housing (plates)	3082.4
damper housing (center)	7035.2
damper MR fluid	891.0
e.e plate	1448.6
damper encoder	292.5
L brackets	953.6
end-effector rod	1497.9
TOTAL, motor side	**15601.6**

Motor Side

Damper Spool:

Material: Steel

Disk portions:

$$J_1 = \frac{1}{2}mr^2 = \frac{1}{2}\rho V\frac{D^2}{4} = \frac{1}{2}\rho\pi\left(\frac{D}{2}\right)^2 l\frac{D^2}{4} = \frac{1}{32}\rho\pi D^4 l$$

$$= \frac{1}{32}(0.28)\pi(2.750)^4(.72) = 2.526 lbm{\bullet}in^2 = 3312 g{\bullet}cm^2$$

Narrow middle:

$$J_2 = \frac{1}{2}mr^2 = \frac{1}{2}\rho V\frac{D^2}{4} = \frac{1}{2}\rho\pi\left(\frac{D}{2}\right)^2 l\frac{D^2}{4} = \frac{1}{32}\rho\pi D^4 l$$

$$= \frac{1}{32}(0.28)\pi(1.33)^4(.72) = 0.06193 lbm{\bullet}in^2 = 181.2 g{\bullet}cm^2$$

Copper Winding:

Material: Copper

$$J_3 = \frac{1}{2}mr^2 = \frac{1}{2}\rho V\frac{D^2}{4} = \frac{1}{2}\rho\pi\left(\frac{D}{2}\right)^2 l\frac{D^2}{4} = \frac{1}{32}\rho\pi D^4 l$$

$$= \frac{1}{32}(0.32)\pi(2.50)^4(.7 \text{ [winding efficiency]})(.72) = 0.6262 lbm{\bullet}in^2 = 1810 g{\bullet}cm^2$$

Total:

$$J_{spool} = J_1 + J_2 + J_3 = 5303 g \bullet cm^2$$

End-Effector Side

Damper Housing, Flanges:

Material: Aluminum

$$J_4 = \frac{1}{2} m r^2 = \frac{1}{2} \rho V \frac{D^2}{4} = \frac{1}{2} \rho \pi \left(\frac{D}{2} \right)^2 l \frac{D^2}{4} = \frac{1}{32} \rho \pi D^4 l$$

$$= \frac{1}{32} (0.098) \pi (1.68)^4 (.375 \bullet 2) = 0.0575 lbm \bullet in^2 = 168.2 g \bullet cm^2$$

Damper Housing, Case:

Material: steel

$$J_5 = \frac{1}{2} m (r_o^{\,2} - r_i)^2 = \frac{1}{2} \rho V \frac{(D_o^{\,2} - D_i^{\,2})}{4} = \frac{1}{2} \rho \pi \frac{(D_o^{\,2} - D_i^{\,2})}{4} l \frac{(D_o^{\,2} + D_i^{\,2})}{4}$$

$$= \frac{1}{32} \rho \pi (D_o^{\,2} - D_i^{\,2})(D_o^{\,2} + D_i^{\,2}) l$$

$$= \frac{1}{32} (0.28) \pi (3.361^2 - 2.986^2)(3.361^2 + 2.986^2)(2.415)$$

$$= 3.630 lbm \bullet in^2 = 10630 g \bullet cm^2$$

Total:

$$J_{ee} = J_4 + J_5 = 10798 g \bullet cm^2$$

Appendix C

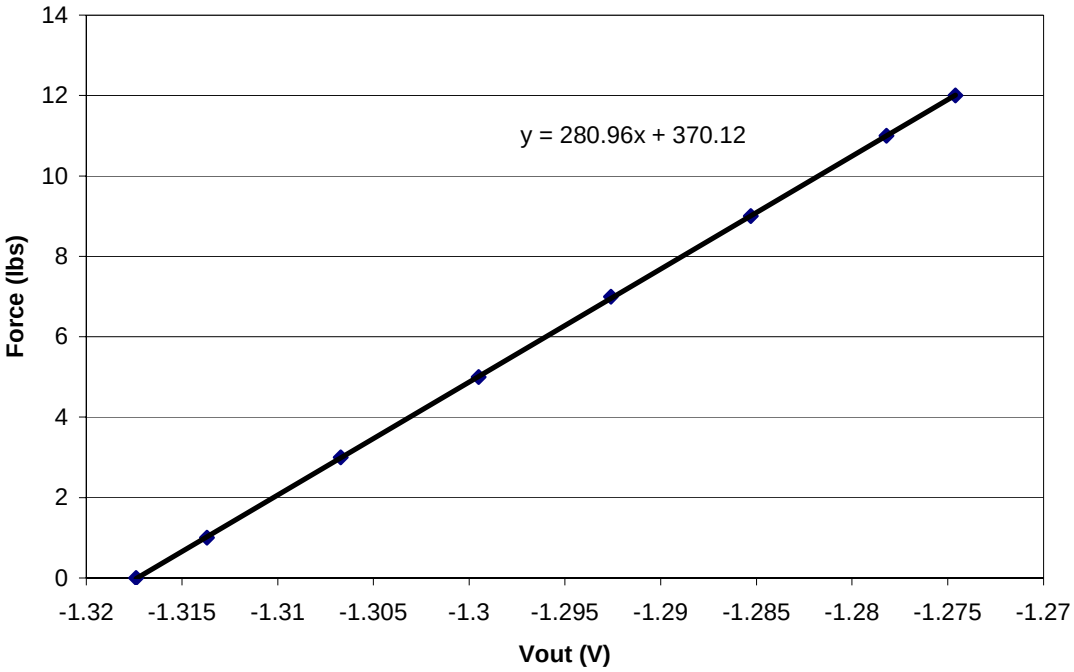

Figure C.1: Calibration curve for model 31/1430-06-04

Appendix D

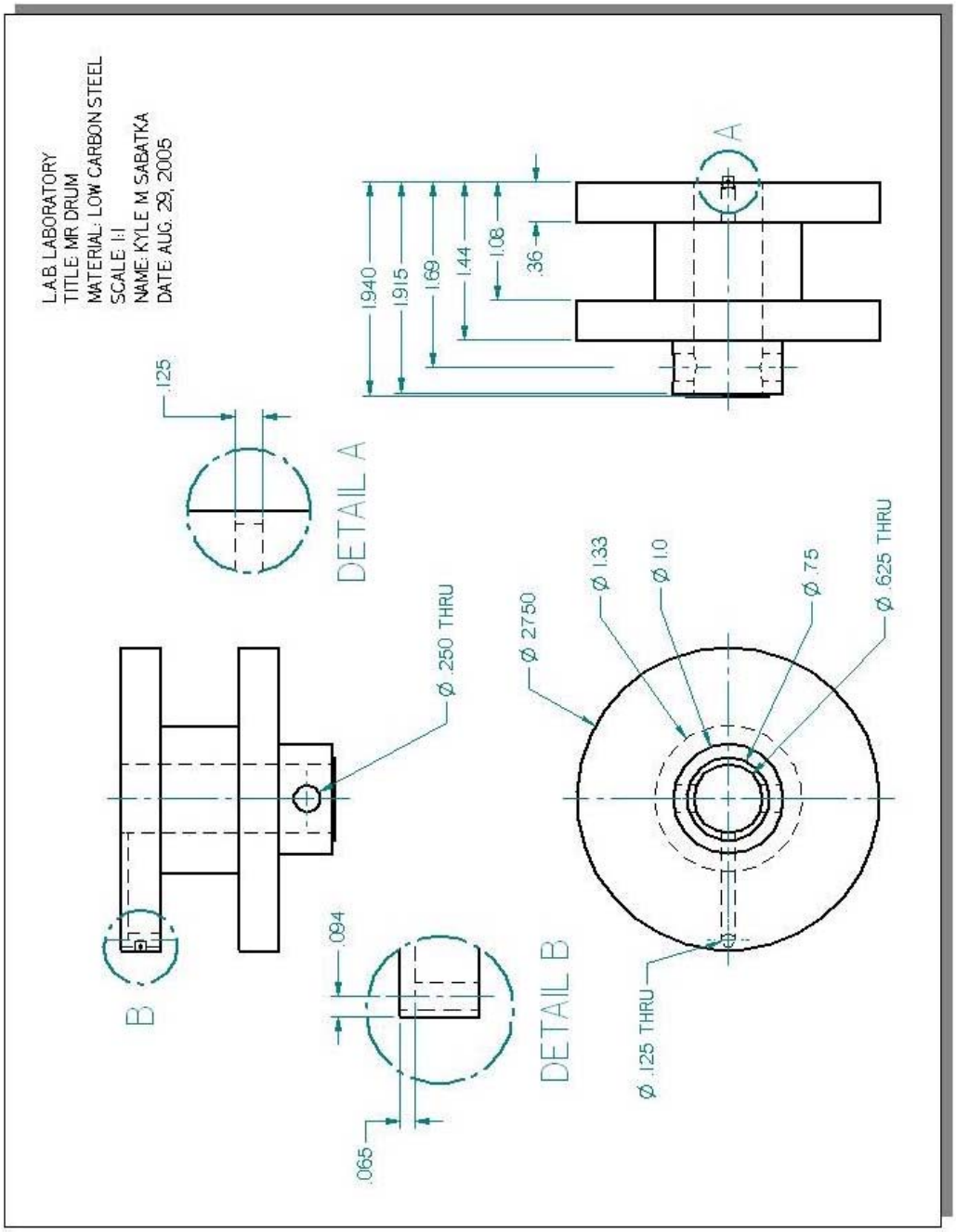
L.A.B. LABORATORY
TITLE: MR DRUM
MATERIAL: LOW CARBON STEEL
SCALE: 1:1
NAME: KYLE M. SABATKA
DATE: AUG. 29, 2005
1.940
1.915
1.69
1.44
1.08
.36
A
.125
DETAIL A
Ø .250 THRU
B
.094
.065
DETAIL B
Ø 2.750
Ø 1.33
Ø 1.0
Ø .75
Ø .625 THRU
Ø .125 THRU

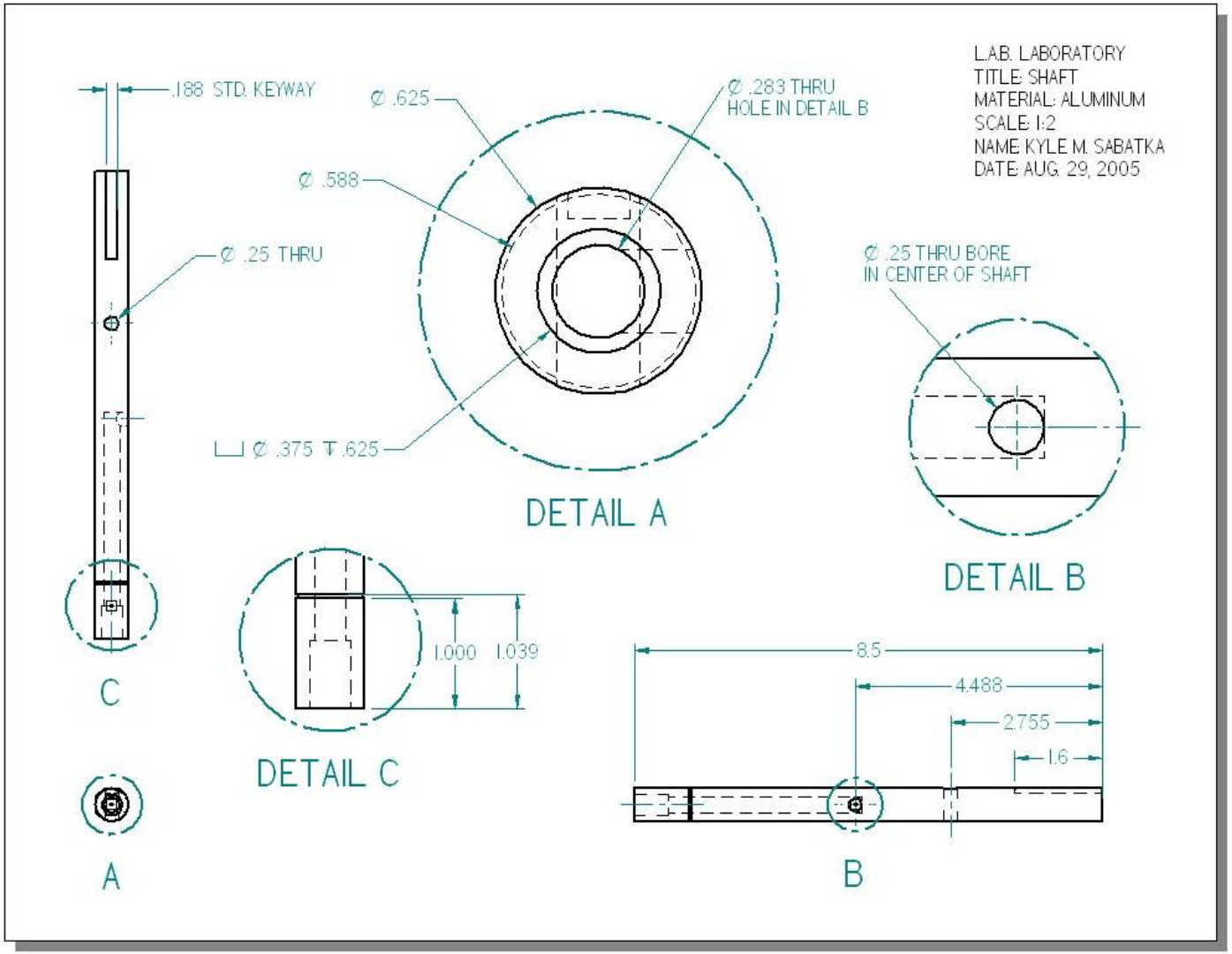
L.A.B. LABORATORY
TITLE: SHAFT
MATERIAL: ALUMINUM
SCALE: 1:2
NAME: KYLE M. SABATKA
DATE: AUG. 29, 2005
.188 STD. KEYWAY
Ø .25 THRU
Ø .625
Ø .588
Ø .283 THRU
HOLE IN DETAIL B
⌴ Ø .375 ↧ .625
DETAIL A
Ø .25 THRU BORE
IN CENTER OF SHAFT
DETAIL B
1.000
1.039
DETAIL C
8.5
4.488
2.755
1.6
C
A
B

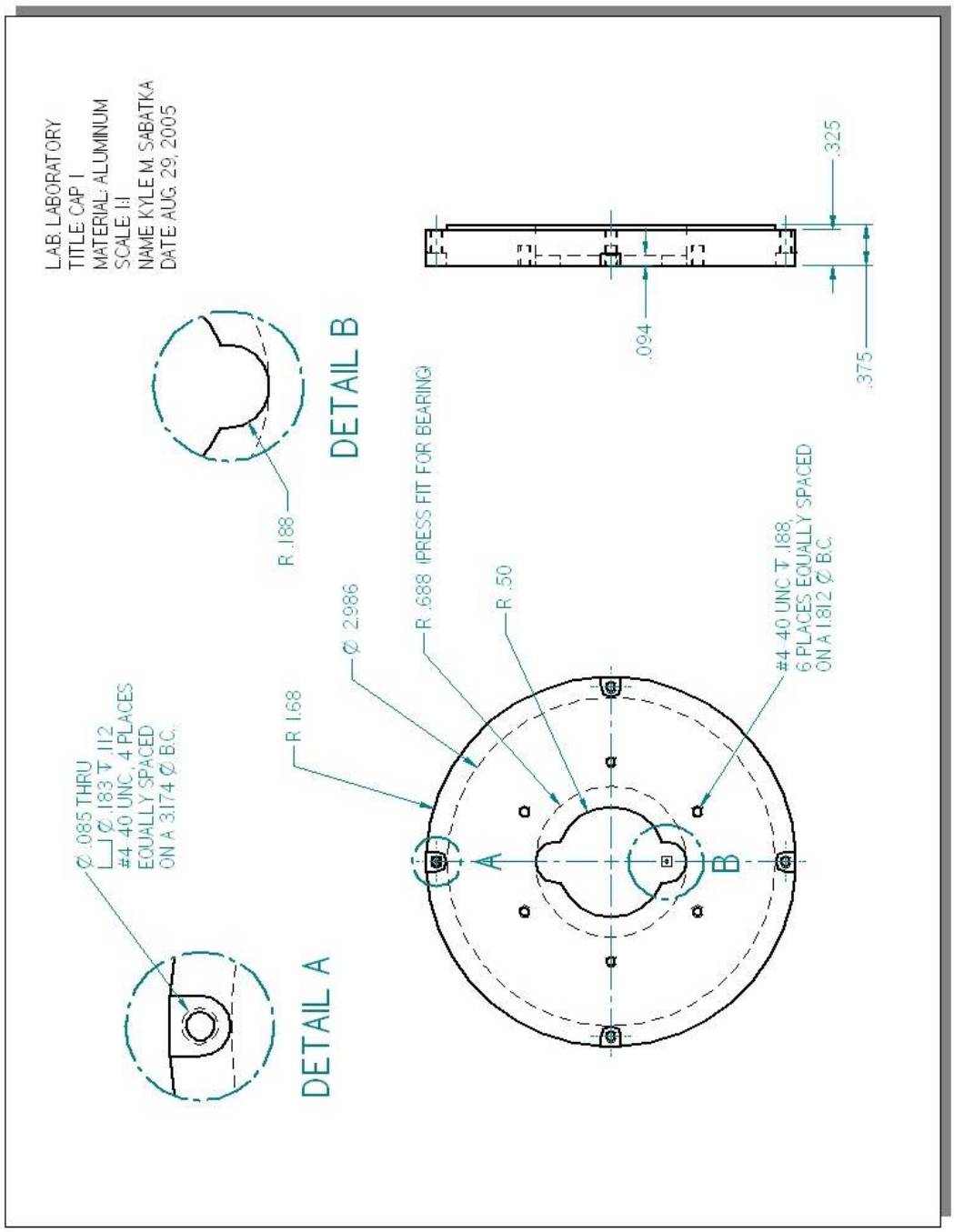
L.A.B. LABORATORY
TITLE: CAP 1
MATERIAL: ALUMINUM
SCALE 1:1
NAME KYLE M. SABATKA
DATE: AUG. 29, 2005
Ø .085 THRU
⌴ Ø .183 ↧ .112
#4 40 UNC, 4 PLACES
EQUALLY SPACED
ON A 3.174 Ø B.C.
DETAIL A
R 1.68
Ø 2.986
R .688 (PRESS FIT FOR BEARING)
R .50
A
B
#4 40 UNC ↧ .188,
6 PLACES EQUALLY SPACED
ON A 1.812 Ø B.C.
R .188
DETAIL B
.094
.325
.375

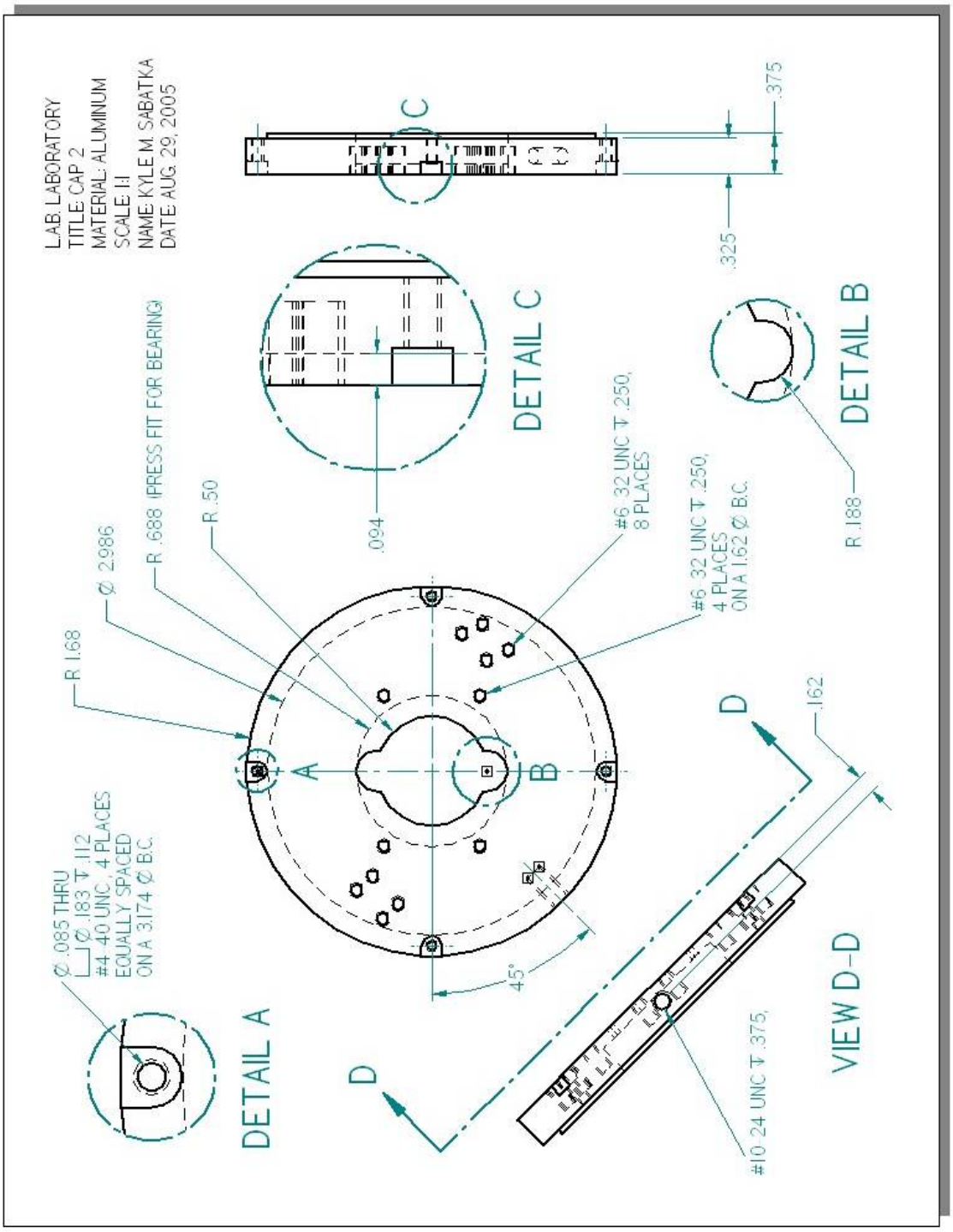
LAB: LABORATORY
TITLE: CAP 2
MATERIAL: ALUMINUM
SCALE: 1:1
NAME: KYLE M. SABATKA
DATE: AUG. 29, 2005
R .50
R .688 (PRESS FIT FOR BEARING)
Ø 2.986
R 1.68
Ø .085 THRU
Ø .183 ↧ .112
#4 40 UNC, 4 PLACES
EQUALLY SPACED
ON A 3.174 Ø B.C.
#6 32 UNC ↧ .250,
8 PLACES
#6 32 UNC ↧ .250,
4 PLACES
ON A 1.62 Ø B.C.
#10 24 UNC ↧ .375,
.094
.325
.375
.162
R .188
45°
A
B
C
D
D
DETAIL A
DETAIL C
DETAIL B
VIEW D-D

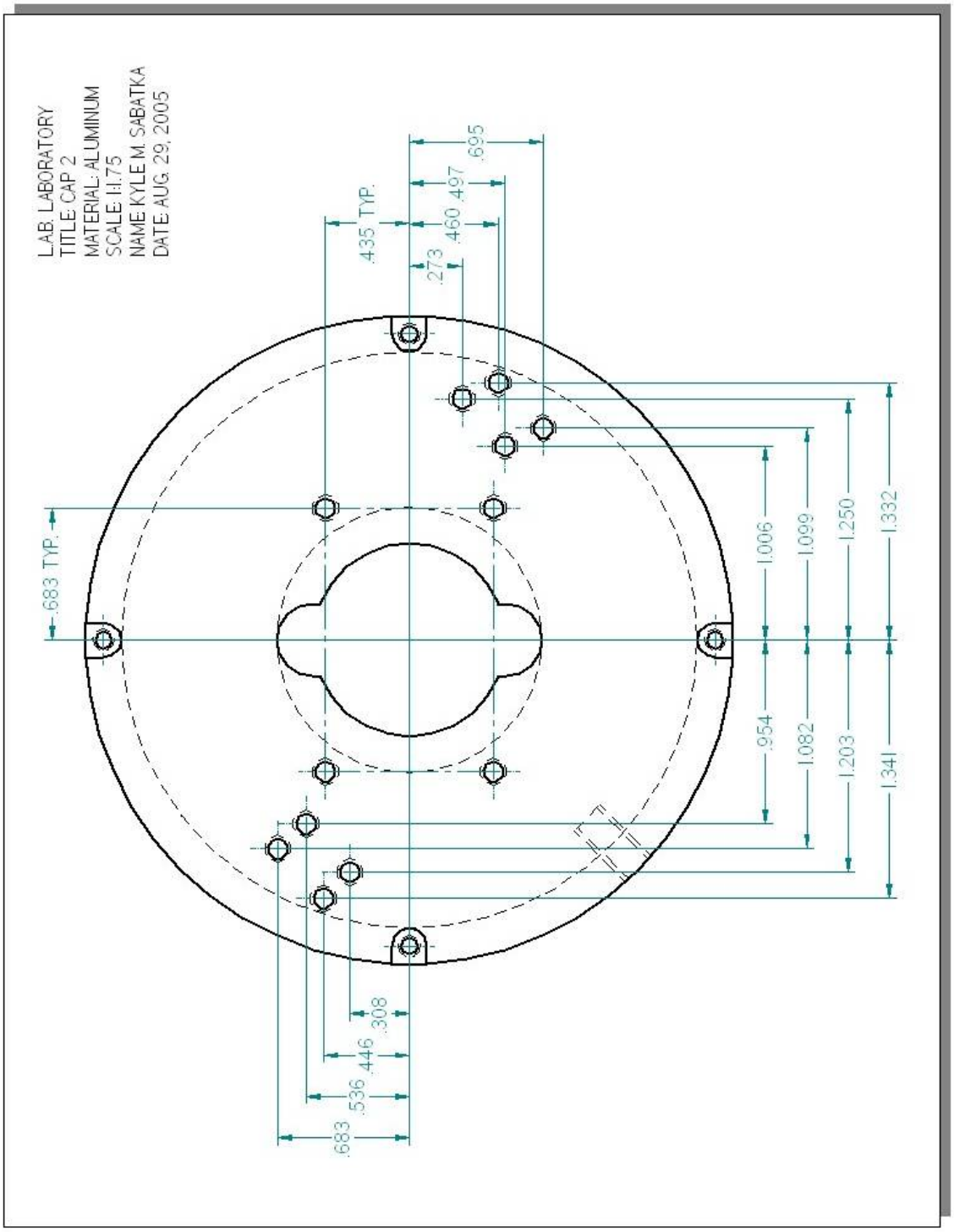
LAB. LABORATORY
TITLE: CAP 2
MATERIAL: ALUMINUM
SCALE: 1:1.75
NAME KYLE M. SABATKA
DATE: AUG. 29, 2005
.683 TYP.
.435 TYP.
.273
.460
.497
.695
.683
.536
.446
.308
.954
1.006
1.082
1.099
1.203
1.250
1.341
1.332

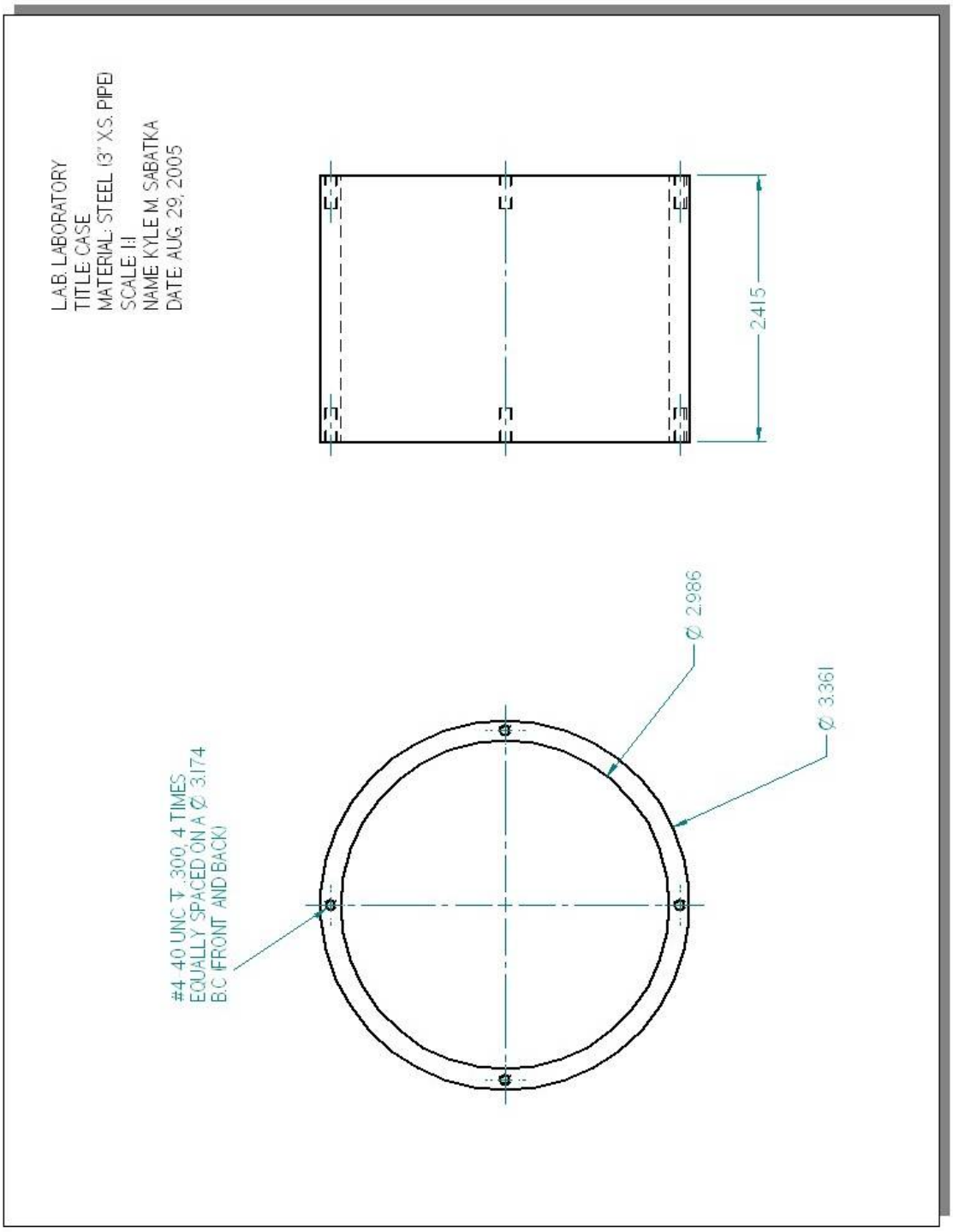
L.A.B. LABORATORY
TITLE: CASE
MATERIAL: STEEL (3" X.S. PIPE)
SCALE: 1:1
NAME: KYLE M. SABATKA
DATE: AUG. 29, 2005
2.415
Ø 2.986
Ø 3.361
#4 40 UNC ↧ .300, 4 TIMES
EQUALLY SPACED ON A Ø 3.174
B.C. (FRONT AND BACK)

LIST OF REFERENCES

Adams, J., Bajcsy, R., Kosecka, J., Kuman, V., Mandelbaum, R., Mintz, M., Paul, R., Wang, C., Yamamoto, Y., & Yun, X. (1995). "Cooperative material handling by human and robotic agents: Module development and system synthesis." *Proceedings of IEEE/RSJ International Conference on Intelligent Robots and Systems*, Pittsburgh, PA, pp. 200-205.

Ahmadkhanlou, Farzad. Personal Communication, 2005.

An, J., & Kwon, D.-S. (2003) "Modeling of a magnetorheological actuator including magnetic hystereis." *Journal of Intelligent Material Systems and Structures*, 14(9), pp. 541-550.

Bicchi, A., Rizzini, S., & Tonietti, G. (2001). "Compliant design for intrinsic safety: general issues and preliminary design." *Proceedings of IEEE/RSJ International Conference on Intelligent Robots and Systems,* Maui, Hawaii, pp 1864-1869.

Bicchi, A. & Tonietti, G. (2004). "Fast and "soft-arm" tactics." *IEEE Robotics & Automation Magazine, 11(2), pp. 22-33.*

Bunting, Tiffany. "Design and Testing of a Variable Effective Compliance Transmission with an MR Damper." Diss. The Ohio State University. 2005.

Chou, C., & Hannaford, B. (1996). "Measurement and modeling of McKibben pneumatic artificial muscles." *IEEE Transactions on Robotics and Automation*, 12(1), pp. 90-102.

Kim, M., Yoon, S.-S., Kanh, S., Kim, S.-J., Kim, Y.-H., Yim, H.-S., Lee, C.-D., & Yeo, I.-T. (2002). "Safe arm design for service robot." *Proceedings of the 2nd IARP-IEEE/RAS Joint Workshop on Technical Challenges for Dependable Robots in Human Environments,* Seoul, Korea, pp. 88-93.

Kim, M., Yun, S., & Kang, S. (2004). "Safe design and vibration control of a manipulator with passive compliant joints." *2nd International Conference on Autonomous Robots and Agents,* Palmerston North, New Zealand, pp. 180-185.

Laurin-Kovitz, K., Colgate, J., & Carnes, S. (1991). "Design of components for programmable passive impedance." *Proceedings of International Conference on Robotics and Automation,* Sacramento, CA., pp 1476-1481.

Morita, T., & Sugano, S. (1995). "Design and development of a new robot joint using a mechanical impedance adjuster." *Proceedings of IEEE Conference on Robotics and Automation*, pp2469-2475.

Pratt, G., & Williamson, M. (1995). "Series elastic actuators." *Proceedings of IEEE/RSJ International Conference on Intelligent Robots and Systems,* Pittsburgh, PA, pp. 399-406.

Pratt, J., & Krupp, B. (2004). "Series elastics actautors for legged robots." *Proceedings of SPIE Conference on Unmanned Ground Vehicle Technology VI.* 5422, pp. 135-144.

Pratt, J., & Pratt, G. (1998). "Intuitive control of a planar bipedal walking robot." *Proceedings of IEEE International Conference on Robotics and Automation.* Leuven, Belgium.

Suzuki, M., Shiller, D., Gribble, P., & Ostry, D. (2001). "Relationship between contraction, movement kinematics and phasic muscle activity in single joint arm movement." *Experimental Brain Research,* 140(2), pp. 171-181.

Takesue, N., Zhang, G., Furusho, J., & Sakaguchi, M. (1999). "Precise position control of robot arms using a homogeneous ER fluid." *IEEE Control Systems Magazine,* 19, pp55-61.

Traver, V., del Pobil, A., & Pérez-Francisco, M. (2000). "Making service robots human-safe." *Proceedings of IEEE/RSJ International Conference on Intelligent Robots and Systems,* pp. 696-701.

Westervelt, E., Schmiedeler, J., & Washington, G. (2004) "Variable transmission compliance with an MR damper." *Proceedings of ASME International Mechanical Engineering Congress and RD&D Expo,* Anaheim, CA.